Remote Sensing of Environment 114 (2010) 2548–2563

Contents lists available at ScienceDirect

Remote Sensing of Environment

journal homepage: www.elsevier.com/locate/rse

# The temporal dimension of differenced Normalized Burn Ratio (dNBR) fire/burn severity studies: The case of the large 2007 Peloponnese wildfires in Greece

S. Veraverbeke [a,*], S. Lhermitte [b], W.W. Verstraeten [c], R. Goossens [a]

[a] Department of Geography, Ghent University, Ghent, Belgium
[b] Centro de Estudios Avanzados en Zonas Aridas (CEAZA), Universidad de la Serena, La Serena, Chile
[c] Geomatics Engineering, Katholieke Universiteit Leuven (K.U.Leuven), Leuven, Belgium

ARTICLE INFO

*Article history:*
Received 27 October 2009
Received in revised form 24 May 2010
Accepted 24 May 2010

*Keywords:*
Fire severity
Burn severity
Differenced Normalized Burn Ratio
MODIS
LANDSAT
Peloponnese
Fire

ABSTRACT

The temporal dimension of differenced Normalized Burn Ratio (dNBR) fire/burn severity studies was studied for the case of the large 2007 Peloponnese wildfires in Greece. Fire severity is defined as the degree of environmental change as measured immediately post-fire, whereas burn severity combines the direct fire impact and ecosystems responses. Geo Composite Burn Index (GeoCBI), two pre-/post-fire differenced Thematic Mapper (TM) dNBR assessments and a Moderate Resolution Imaging Spectroradiometer (MODIS) dNBR time series were used to analyze the temporal dimension. MODIS dNBR time series were calculated based on the difference between the NBR of the burned and control pixels, which were retrieved using time series similarity of a pre-fire year. The analysis incorporated the optimality statistic, which evaluates index performance based on displacements in the mid-infrared–near infrared bi-spectral space. Results showed a higher correlation between field and TM data early post-fire ($R^2 = 0.72$) than one-year post-fire ($R^2 = 0.56$). Additionally, mean dNBR (0.56 vs. 0.29), the dNBR standard deviation (0.29 vs. 0.19) and mean optimality (0.65 vs. 0.47) were clearly higher for the initial assessment than for the extended assessment. This is due to regenerative processes that obscured first-order fire effects impacting the suitability of the dNBR to assess burn severity in this case study. This demonstrates the importance of the lag timing, i.e. time since fire, of an assessment, especially in a quickly recovering Mediterranean ecosystem. The MODIS time series was used to study intra-annual changes in index performance. The seasonal timing of an assessment highly impacts what is actually measured. This seasonality affected both the greenness of herbaceous resprouters and the productivity of the control pixels, which is land cover specific. Appropriate seasonal timing of an assessment is therefore of paramount importance to anticipate false trends (e.g. caused by senescence). Although these findings are case study specific, it can be expected that similar temporal constraints affect assessments in other ecoregions. Therefore, within the limitations of available Landsat imagery, caution is recommended for the temporal dimension when assessing post-fire effects. This is crucial, especially for studies that aim to evaluate trends in fire/burn severity across space and time. Also, clarification in associated terminology is suggested.



## 1. Introduction

Wildfires affect the ecological functioning of many ecosystems (Dwyer et al., 1999; Pausas, 2004; Riano et al., 2007) as they partially or completely remove the vegetation layer and affect post-fire vegetation composition (Epting & Verbyla, 2005; Lentile et al., 2005). They act as a natural component in vegetation succession cycles (Capitaino & Carcaillet, 2008; Roder et al., 2008; Trabaud, 1981) but also potentially increase degradation processes, such as soil erosion (Chafer, 2008; Fox et al., 2008; Perez-Cabello et al., 2006; Thomas et al., 1999). Assessment of post-fire effects is thus a major challenge to understand the potential degradation after fire (Fox et al., 2008; Kutiel & Inbar, 1993) and to comprehend the ecosystem's post-fire resilience (Epting & Verbyla, 2005; Lentile et al., 2005).

The fire impact can be described as (i) the amount of damage (Chafer, 2008; Gonzalez-Alonso et al., 2007; Hammill & Bradstock, 2006), (ii) the physical, chemical and biological changes (Chafer et al., 2004; Cocke et al., 2005; Landmann, 2003; Lee et al., 2008; Stow et al., 2007) or (iii) the degree of alteration (Brewer et al., 2005; Eidenshink et al., 2007) that fire causes to an ecosystem and is quantified as the severity of fire. In this context the terms fire severity and burn severity are often interchangeably used (Keeley, 2009). Lentile et al. (2006), however, suggest a clear distinction between both terms by considering the fire disturbance continuum (Jain et al., 2004), which addresses three different temporal fire effects phases: before, during and after the fire. In this framework fire severity quantifies the short-

* Corresponding author.
*E-mail address:* sander.veraverbeke@ugent.be (S. Veraverbeke).

0034-4257/$ – see front matter © 2010 Elsevier Inc. All rights reserved.
doi:10.1016/j.rse.2010.05.029

term fire effects in the immediate post-fire environment while burn severity quantifies both the short- and long-term impact as it includes response processes. While this substantive difference in terminology between fire and burn severity is generally accepted in the remote sensing community, fire ecologists tend to smooth away this distinction as they opt to exclude ecosystem responses from the term burn severity (Keeley, 2009), thereby reducing its meaning to the same dimension as the term fire severity, which makes both terms mutually substitutional. However, the inclusion of ecosystem responses (such as regrowth, regeneration and resilience) in burn severity is justified by the significant negative correlation between direct fire impact and regeneration ability (Diaz-Delgado et al., 2003). Moreover, except for assessments immediately post-fire (within the first month), ecosystem responses cannot be neglected in a satellite assessment as it is practically infeasible to uncouple these effects from the direct fire impact based on the image data. In addition, Key and Benson (2005) and Key (2006) introduced three sets of complementary concepts. The first set differentiates between first- and second-order effects, where first-order effects are caused by the fire only, whereas second-order effects also involve other causal agents (e.g. wind, rain, vegetative processes, etc.). Secondly, short-and long-term severity refer to the condition of the burned area. Short-term severity is restricted to the pre-recovery phase, while long-term severity includes both first- and second-order effects. Thirdly, Key (2006) differentiates between an initial assessment (IA) and an extended assessment (EA). This difference results from differing lag timing, i.e. the time since fire, on which an assessment is made. An IA is executed immediately after the fire event, whereas by EAs a certain amount of time elapses between the fire event and the assessment. Summarized, fire severity is defined as the degree of environmental change caused by fire and is related to first-order effects, short-term severity and IAs (Key & Benson, 2005). As such it mainly quantifies vegetation consumption and soil alteration. Burn severity, on the other hand, is equally defined as the degree of environmental change caused by fire, but it also includes second-order effects (e.g. resprouting, delayed mortality, etc.), long-term severity and is usually measured in an EA (Key & Benson, 2005). Finally, the term post-fire effects (Lentile et al., 2006) groups all above mentioned severity-related notions. In Fig. 1 a schematic representation of post-fire effects terminology is given.

Even though a considerable amount of remote sensing studies have focused on the use of the Normalized Difference Vegetation Index (NDVI) for assessing burn severity (Chafer et al., 2004; Diaz-Delgado et al., 2003; Hammill & Bradstock, 2006; Hudak et al., 2007; Isaev et al., 2002; Ruiz-Gallardo et al., 2004), the Normalized Burn Ratio (NBR) has become accepted as the standard spectral index to estimate fire/burn severity (e.g. Bisson et al., 2008; Epting et al., 2005; Key & Benson, 2005; Lopez-Garcia & Caselles, 1991; Veraverbeke et al., in press—a,b). The NBR is used as an operational tool at national scale in the United States (Eidenshink et al., 2007). The index relates to vegetation vigor and moisture by combining near infrared (NIR) and mid-infrared (MIR) reflectance and is defined as:

$$NBR = \frac{NIR - MIR}{NIR + MIR}. \quad (1)$$

Most of the studies that assessed burn severity were conducted with Landsat imagery (French et al., 2008), thanks to Landsat's unique properties of operating a MIR band and a desirable 30 m resolution for local scale studies. Since fire effects on vegetation produce a reflectance increase in the MIR spectral region and a NIR reflectance drop (Key, 2006; Pereira et al., 1999), bi-temporal image differencing is frequently applied on pre- and post-fire NBR images resulting in the differenced Normalized Burn Ratio (dNBR) (Key & Benson, 2005). Additionally, Miller and Thode (2007) proposed a relative version of the dNBR (RdNBR). This index takes into account the pre-fire amount of biomass, and therefore, rather than being a measure of absolute change, reflects the change caused by fire relative to the pre-fire condition. Apart from the correlation with field data (De Santis & Chuvieco, 2009; Key & Benson, 2005; Veraverbeke et al., in press—a,b), the performance of bi-spectral indices can be evaluated by assessing a pixel's shift in the bi-spectral feature space. As such, a pixel-based optimality measure, originating from the spectral index theory (Verstraete & Pinty, 1996), has been developed by Roy et al. (2006). They used the optimality concept to question the dNBR method as an optimal fire/burn severity approach. The optimality value varies between zero (not at all optimal) and one (fully optimal). An optimal fire/burn severity spectral index needs to be as insensitive as possible to perturbing factors, such as atmospheric and illumination effects

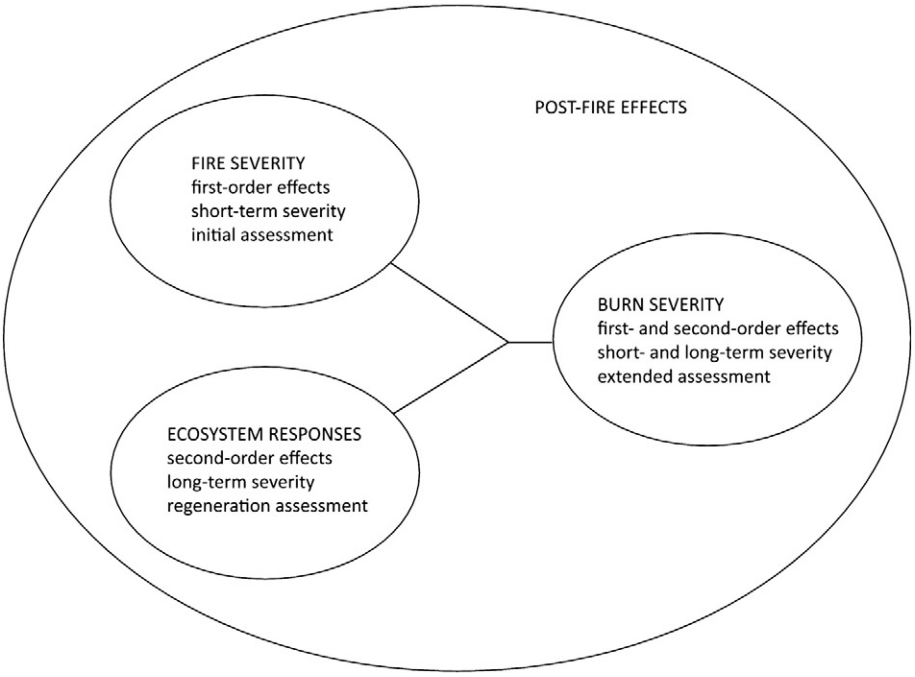


**Fig. 1.** Schematic representation of post-fire effects terminology.

(Veraverbeke et al., 2010), and highly sensitive to fire-induced vegetation changes.

These post-fire vegetation changes typically are abrupt immediately after fire (Pereira et al., 1999), whereas a more gradual and progressive vegetation regeneration process is initiated several weeks after the fire (Viedma et al., 1997; van Leeuwen, 2008). Despite of the current discussion on the temporal dimension in fire/burn severity studies (Keeley, 2009) (see Fig. 1), relatively few studies have addressed attention to the influence of assessment timing on the estimation of post-fire effects. In this respect Key (2006) comprehensively differentiates between two temporal constraints. The first constraint is the lag timing. IAs focus on the first opportunity to get an ecological evaluation of within-burn differences in combustion completeness, whereas EAs occur as a rule in the first post-fire growing season (Key, 2006). This constraint especially becomes obvious in quickly recovering ecosystems where an inappropriate lag timing can distort or hide the fire effects (Allen & Sorbel, 2008; Lhermitte et al., submitted for publication). Allen and Sorbel (2008), for example, found that IA and EA produced significantly different information for tundra vegetation, while the timing of the assessment had no effect for black spruce forest. This was attributed to the rapid tundra recovery (Allen & Sorbel, 2008). The second constraint deals with the seasonal timing, i.e. the biophysical conditions that vary throughout the year, regardless of the fire. Analysis shortly after the usually dry fire season for example can be detracted because of the reduced variability in vegetation vigor during the dry season. Conversely, when vegetation is green and productive, a broader range of severity can be detected with better contrast (Key, 2006). The importance of the phenological timing of an assessment was also pointed by Verbyla et al. (2008). They found a clear discrepancy in dNBR values between two different Landsat assessments, which was partly attributed to the seasonal timing of the bi-temporal acquisition scheme, while another part of the difference was due to the changing solar elevation angles at the moment of the image acquisition. Apart from these studies, relatively little attention has been devoted to the temporal changes in the NBR and its consequence to estimate fire/burn severity. This is probably due to the 16-day repeat cycle of Landsat and the problem of cloudiness which restricts image availability to infrequent images over small areas (Ju & Roy, 2008). Multi-temporal Moderate Resolution Imaging Spectroradiometer (MODIS) data can bridge the gap of image availability. MODIS is the only high temporal-frequent coarse resolution (500 m) sensor which has the spectral capability, i.e. acquisition of reflectance data in the MIR region besides to the NIR region (Justice et al., 2002), to calculate the NBR. MODIS surface reflectance data (Vermote et al., 2002) are therefore an ideal source of information to explore the post-fire temporal, both in terms of lag and seasonal timing, sensitivity of the dNBR to assess fire/burn severity.

Hence, the general objective of this paper is assessing the temporal dimension of the dNBR and its consequence for the estimation of fire/burn severity of the large 2007 Peloponnese wildfires in Greece. This objective is fulfilled by evaluating (i) the relationship between field data of severity, Landsat dNBR and MODIS dNBR for an IA and EA scheme, and (ii) the one-year post-fire temporal changes in dNBR and dNBR optimality for different fuel types. 500 m MODIS dNBR data are used in this study as a way to explore the temporal dimension, not as a substitute for 30 m Landsat dNBR imagery which is superior for spatial detail (French et al., 2008).

## 2. Data and study area

### 2.1. Study area

The study area is situated at the Peloponnese peninsula, in southern Greece (36°30′–38°30′ N, 21°–23° E) (see Fig. 2). The topography is rugged with elevations ranging between 0 and 2404 m above sea level.

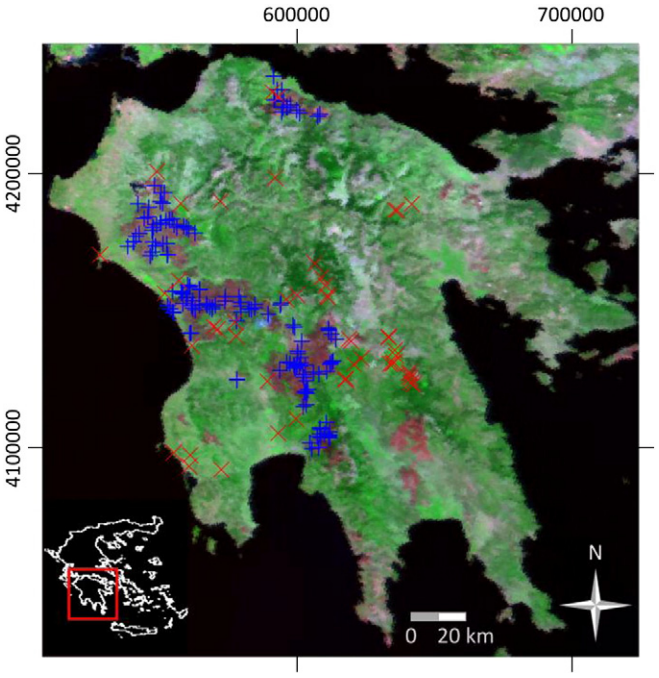


**Fig. 2.** Location of the study area (MODIS daily surface reflectance MOD09GA FCC 01/09/2007 RGB-721, UTM 34 S WGS84). Blue crosses indicate the field plot distribution (section 2.2), while red crosses show the locations of the training samples used in the land cover classification (Section 3.1).

The climate is typically Mediterranean with hot, dry summers and mild, wet winters (see Fig. 3). For the Kalamata meteorological station (37°4′ N, 22°1′ E) the average annual temperature is 17.8 °C and the mean annual precipitation equals 780 mm.

After a severe drought period several large wildfires of unknown cause have struck the area in August 2007. The fires consumed more than 150,000 ha of coniferous forest, broadleaved forest, shrub lands (maquis and phrygana communities) and olive groves. Black pine (*Pinus nigra*) is the dominant conifer species. Maquis communities consist of sclerophyllous evergreen shrubs of 2–3 m high (Polunin, 1980). Phrygana is dwarf scrub vegetation (<1 m), which prevails on dry landforms (Polunin, 1980). The shrub layer is characterized by e.g. *Quercus coccifera, Q. frainetto, Pistacia lentiscus, Cistus salvifolius, C. incanus, Erica arborea, Sarcopoterum spinosum*. The olive groves consist of *Olea europaea* trees, whereas oaks are the dominant broadleaved species.

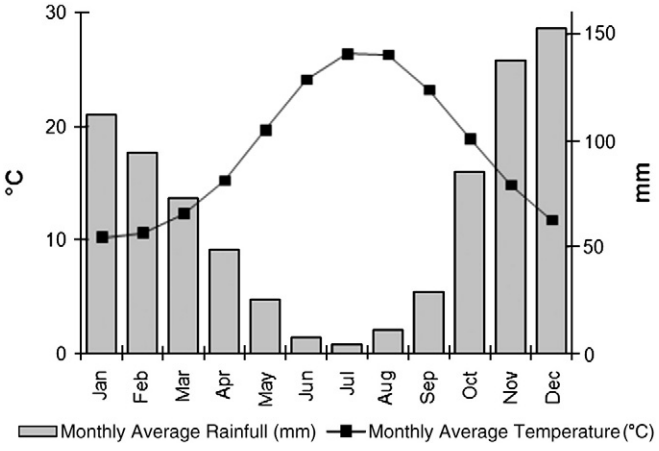


**Fig. 3.** Ombrothermic diagram of the Kalamata (Peloponnese, Greece) meteorological station (37°4′1″ N 22°1′1″ E) 1956–1997 (Hellenic National Meteorological Service, www.hnms.gr).

### 2.2. Field data

To assess fire/burn severity in the field, 150 Geo Composite Burn Index (GeoCBI) plots were collected one-year post-fire, in September 2008 (see Fig. 2). The GeoCBI is a modified version of the Composite Burn Index (CBI) (De Santis & Chuvieco, 2009). The (Geo)CBI is an operational tool used in conjunction with the Landsat dNBR approach to assess fire/burn severity in the field (Key & Benson, 2005). The GeoCBI divides the ecosystem into five different strata, one for the substrates and four vegetation layers. These strata are: (i) substrates, (ii) herbs, low shrubs and trees less than 1 m, (iii) tall shrubs and trees of 1 to 5 m, (iv) intermediate trees of 5 to 20 m and (v) big trees higher than 20 m. In the field form, 20 different factors can be rated (e.g. soil and rock cover/color change,% LAI change, char height) (see Table 1) but only those factors present and reliably rateable, are considered. The rates are given on a continuous scale between zero and three and the resulting factor ratings are averaged per stratum. Based on these stratum averages, the GeoCBI is calculated in proportion to their corresponding fraction of cover, resulting in a weighted average between zero and three that expresses burn severity. As the field data were collected one-year post-fire, it is an EA. We believe that the direct fire effects visible in the plots would not have lead to significantly different ratings when IA and EA schemes would have been sampled independently. However, it is obvious to omit the factor new sprouts form the IA scheme as this factor is not relevant in a fire severity assessment (see Fig. 1) because regeneration processes have not yet started at that moment.

The 150 sample points were selected based on a stratified sampling approach, taking into account the constraints on mainly accessibility and time, which encompasses the whole range of variation found within the burns. The field plots consist of 30 by 30 m squares, analogous to the Landsat pixel size. The pixel centre coordinates were recorded based on measurements with a handheld Garmin eTrex Vista Global Positioning System (15 m error in x and y (Garmin, 2005)) device. To minimize the effect of potential misregistration, plots were at least 90 m apart and chosen in relatively homogeneous areas (Key & Benson, 2005). This homogeneity refers both to the fuel type (homogeneity of at least 500 m) and the fire effects (homogeneity of at least 60 m). Of the 150 field plots 63 plots were measured in shrub land, 57 in coniferous forest, 16 in deciduous forest and 14 in olive groves. More information on the field sampling scheme can be found in Veraverbeke et al. (in press—a,b).

Additionally, 50 training samples in very homogeneous covers (homogeneity of at least 2000 m) were GPS-recorded outside the burned area (see Fig. 2). These samples comprised the most prevailing fuel types in the burned area; 12 samples were taken in coniferous forest, 17 in shrub land, 10 in deciduous forest and 11 in olive groves. The dominant species of these land cover types are given in Section 2.1.

### 2.3. Landsat thematic mapper data

For the traditional Landsat post-fire effects assessment of the summer 2007 Peloponnese fires three anniversary date Landsat Thematic Mapper (TM) images (path/row 184/34) were used (23/07/2006, 28/09/2007 and 13/08/2008). The images were acquired in the summer, minimizing effects of vegetation phenology and differing solar zenith angles. The images were subjected to geometric, radiometric, atmospheric and topographic correction.

The 2008 image was geometrically corrected using 34 ground control points (GCPs), recorded in the field with a Garmin eTrex Vista GPS. The resulting Root Mean Squared Error (RMSE) was lower than 0.5 pixels. The 2006, 2007 and 2008 images were co-registered within 0.5 pixels accuracy. All images were registered in UTM (Universal Transverse Mercator) (zone 34 S), with WGS 84 (World Geodetic System 84) as geodetic datum.

Raw digital numbers (DNs) were scaled to at-sensor radiance values using the procedure of Chander et al. (2007). The radiance to reflectance conversion was performed using the COST method of Chavez (1996). The COST method is a dark object subtraction (DOS) approach that assumes 1% surface reflectance for dark objects (e.g. deep water). After applying the COST atmospheric correction, pseudo-invariant features (PIFs) such as deep water and bare soil pixels, were examined in the images. No further relative normalization between the images was required.

Additionally, it was necessary to correct for different illumination effects due to topography as the common assumption that shading

**Table 1**
GeoCBI criteria used to estimate fire/burn severity in the field (after De Santis & Chuvieco, 2009).

| Stratum | Burn severity scale | | | | | | |
|---|---|---|---|---|---|---|---|
| | No effect | Low | | Moderate | | High | |
| | 0 | 0.5 | 1 | 1.5 | 2 | 2.5 | 3 |
| Substrates | | | | FCOV | | | |
| Litter (l)/light fuel (lf) consumed | 0% | – | 50% l | – | 100% l | >80% lf | 98% lf |
| Duff | 0% | – | Light char | – | 50% | – | Consumed |
| Medium/heavy fuel | 0% | – | 20% | – | 40% | – | >60% |
| Soil & rock cover/color | 0% | – | 10% | – | 40% | – | >80% |
| Herbs, low shrubs and trees less than 1 m | | | | FCOV | | | |
| % Foliage altered | 0% | – | 30% | – | 80% | 95% | 100% |
| Frequency% living | 100% | – | 90% | – | 50% | <20% | 0% |
| New sprouts | Abundant | – | Moderate–high | – | Moderate | – | Low–none |
| Tall shrubs and trees 1 to 5 m | | | | FCOV | | | |
| % Foliage altered | 0% | – | 20% | – | 60–90% | >95% | branch loss |
| Frequency% living | 100% | – | 90% | – | 30% | <15% | <1% |
| LAI change% | 0% | – | 15% | – | 70% | 90% | 100% |
| Intermediate trees 5 to 20 m | | | | FCOV | | | |
| % Green (unaltered) | 100% | – | 80% | – | 40% | <10% | none |
| % Black/brown | 0% | – | 20% | – | 60–90% | >95% | branch loss |
| Frequency% living | 100% | – | 90% | – | 30% | <15% | <1% |
| LAI change% | 0% | – | 15% | – | 70% | 90% | 100% |
| Char height | none | – | 1.5 m | – | 2.8 m | – | >5 m |
| Big trees >20 m | | | | FCOV | | | |
| % Green (unaltered) | 100% | – | 80% | – | 50% | <10% | none |
| % Black/brown | 0% | – | 20% | – | 60–90% | >95% | branch loss |
| Frequency% living | 100% | – | 90% | – | 30% | <15% | <1% |
| LAI change% | 0% | – | 15% | – | 70% | 90% | 100% |
| Char height | none | – | 1.8 m | – | 4 m | – | >7 m |

effects are removed in ratio-based analyses does not necessarily hold true (Veraverbeke et al., 2010; Verbyla et al., 2008). This was done based on the modified c-correction method (Veraverbeke et al., 2010), a modification of the original c-correction approach (Teillet et al., 1982), using a digital elevation model (DEM) and knowledge of the solar zenith and azimuth angle at the moment of image acquisition. Topographical slope and aspect data were derived from 90 m SRTM (Shuttle Radar Topography Mission) elevation data (Jarvis et al., 2006) resampled and co-registered with the TM images.

Finally, by inputting the NIR (TM4: centered at 830 nm) and MIR (TM7: centered at 2215 nm) bands in Eq (1) NBR images were generated.

### 2.4. Moderate Resolution Imaging Spectroradiometer data

Level 2 daily Terra MODIS surface reflectance (500 m) tiles that cover the study area (MOD09GA) including associated Quality Assurance (QA) layers were acquired from the National Aeronautics and Space Administration (NASA) Warehouse Inventory Search Tool (WIST) (https://wist.echo.nasa.gov) for the period 01/01/2006 till 31/12/2008. These products contain an estimate of the surface reflectance for seven optical bands as it would have been measured at ground level as if there were no atmospheric scattering or absorption (Vermote et al., 2002). The data preprocessing steps included subsetting, reprojecting, compositing, creating continuous time series and indexing. The study area was clipped and the NIR (centered at 858 nm), MIR (centered at 2130 nm) and QA layers were reprojected into UTM with WGS 84 as geodetic datum. Subsequently, the daily NIR, MIR and QA data were converted in 8-day composites using the minimum NIR criterion to minimize cloud contamination and off-nadir viewing effects (Holben, 1986). The minimum NIR criterion has proven to allow a more accurate discrimination between burned and unburned pixels than traditional Maximum Value Composites (MVCs) (Barbosa et al., 1998; Chuvieco et al., 2005; Stroppiana et al., 2002). Thus, for each 8-day period the NIR, MIR and QA data were saved corresponding with the minimum NIR observation for each pixel. An additional advantage of the minimum NIR criterion in comparison with MVCs is its tendency to select close to nadir observations (Stroppiana et al., 2002), because for smaller view angles the soil fraction in the vegetation–soil matrix will have a relatively higher contribution to the reflectance signal than for wider viewing angles. After the compositing procedure a minority of the data still lacked good quality values. Therefore, to create continuous time series, a local second-order polynomial function, also known as an adaptive Savitzky–Golay filter (Savitzky & Golay, 1964), was applied to the time series as implemented in the TIMESAT software (Jonsson & Eklundh, 2004) to replace the affected observations. Although other smoothing methods based on for example Fourier series (Olsson & Eklundh, 1994) or least-squares fitting to sinusoidal functions (Cihlar, 1996) are known to work well in most instances, they fail to capture a sudden steep change in remote sensing values, as it is the case in burned land applications (Verbesselt et al., 2006). The TIMESAT program allows the inclusion of a preprocessing mask. These masks are translated into weights, zero and one, that determine the uncertainty of the data values. Cloud-affected observations were identified using the internal cloud and cloud-adjacency algorithm flags of the QA layer. These flags consist of binary layers which permit to assign a zero weight value to cloudy and cloud-adjacent observations. Consequently these data do not influence the filter procedure. Only the values of the masked observations were replaced to retain as much as possible the original NIR and MIR reflectance values. Finally, NBR images were calculated based on Eq. (1).

## 3. Methodology

### 3.1. MODIS pre-fire land cover map

As phenology, fire impact and regeneration typically vary by land cover type (Reed et al., 1994; Viedma et al., 1997; White et al., 1996) the pre-fire land cover of the burned areas was classified. This was done based on the time series similarity concept as phenological differences in time series allow to discriminate different land cover types (Geerken et al., 2005; Lhermitte et al., 2008; Reed et al., 1994; Viovy, 2000). A maximum likelihood classification was performed on a MODIS NBR time series of the pre-fire year 2006. The GPS-recorded pixel and its bilinear neighbors of the 50 land cover field samples (see Section 2.2 and Fig. 3) served as training pixels in the classification. As such the four main land covers (shrub land, coniferous forest, deciduous forest and olive groves) were classified. Fig. 4 displays the mean temporal profiles of the training pixels for each class. Fig. 4A–C, respectively of shrub land, coniferous forest and olive groves, reveal characteristic temporal profiles for evergreen Mediterranean species. For these land cover types seasonal fluctuations are minor. Coniferous forests are characterized by a higher overall productivity than shrub lands and olive groves. Shrub lands reveal a peak in late spring/early summer, which is characteristic for Mediterranean xerophytic species (Maselli, 2004; Specht, 1981). The olive groves are slightly more productive during the winter season, which can be contributed to the favorable moisture conditions during the wet winter months (see Fig. 3). The temporal profile of deciduous forest (Fig. 4D) contrasts with those of evergreen species as it shows a markedly higher seasonality with a summer maximum and winter minimum. The accuracy of the pre-fire land cover map was verified by the 150 GeoCBI field plots with known pre-fire land cover type. These plots were taken in areas that were homogeneous in pre-fire fuel type for at least 500 m.

### 3.2. MODIS control pixel selection

Traditionally fire/burn severity is estimated from pre-/post-fire differenced imagery (French et al., 2008; Key & Benson, 2005). This bi-temporal analysis method can be hampered by phenological effects, both due to the differences in acquisition data and due to inter-annual meteorological variability (Diaz-Delgado & Pons, 2001). To deal with these phenological effects Diaz-Delgado and Pons (2001) proposed to compare vegetation regrowth in a burned area with unburned reference plots within the same image. As such, external and phenological variations are minimized among the compared areas. The reference plot selection procedure has, however, two main difficulties. Firstly, large scale application remains constrained due to the necessity of profound field knowledge to select relevant control plots. Secondly, the reference plot approach fails to describe within-burn heterogeneity as it uses mean values per fire plot. To solve these problems, Lhermitte et al. (2010) proposed a pixel-based control plot selection method which follows the same reasoning with respect to the minimization of phenological effects by comparison with image-based control plots. The difference with the reference plot procedure, however, is situated in the fact that the pixel-based method assigns a unique unburned control pixel to each burned pixel. This control pixel selection is based on the similarity between the time series of the burned pixel and the time series of its surrounding unburned pixels for a pre-fire year (Lhermitte et al., 2010). The method allows to quantify the heterogeneity within a fire plot since each fire pixel is considered independently as a focal study pixel and a control pixel is selected from a contextual neighborhood around the focal pixel. In this study, the procedure of Lhermitte et al. (2010) is followed as it allows exploring the temporal dimension of post-fire effects without image-to-image phenological constraints. The selection is based on the similarity of MODIS NBR time series between pixels during the pre-fire year 2006. The averaged Euclidian distance dissimilarity criterion $D$ was used:

$$D = \frac{\sqrt{\sum_{t=1}^{N}\left(NBR_t^f - NBR_t^x\right)^2}}{N} \quad (2)$$

where $NBR_t^f$ and $NBR_t^x$ are the respective burned focal and unburned candidate control pixel time series, while $N$ is the number of observations

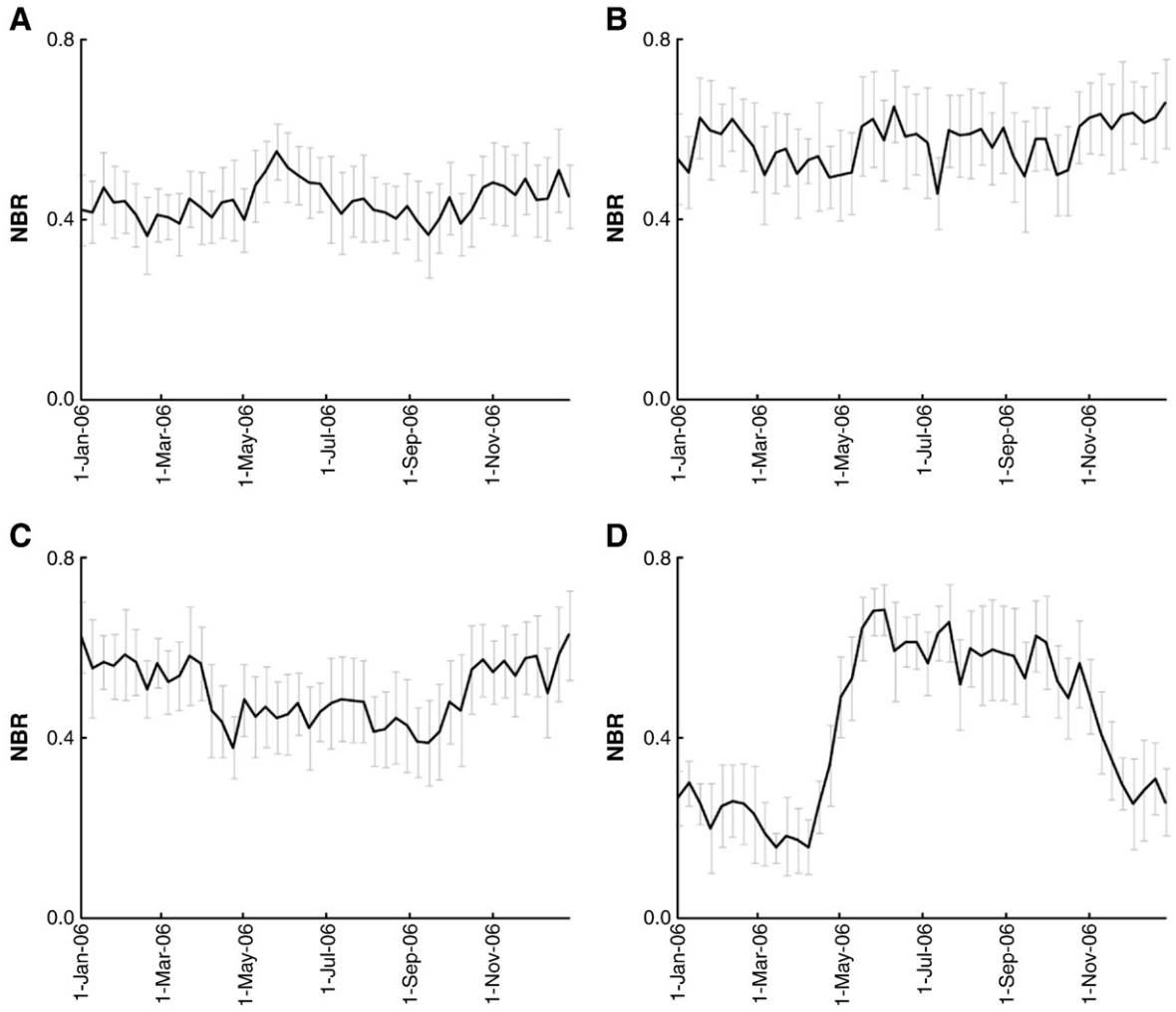


**Fig. 4.** Mean temporal profile (± sd) of (A) shrub land, (B) coniferous forest, (C) olive groves and (D) deciduous forest training samples used in the pre-fire land cover classification.

in pre-fire year ($N = 46$). The Euclidian distance metric has an intuitive appeal: it quantifies the straight line inter-point distance in a multi-temporal space as distance measure. As a result, it is robust for both data space translations and rotations. Consequently, it is a very useful metric to assess inter-pixel differences in time series (Lhermitte et al., 2010). The discrimination between burned and unburned pixels was based on a burned area map. This burned area map was extracted making use of the characteristic persistency of the post-fire NBR drop, similar to the algorithms of Kasischke and French (1995), Barbosa et al. (1999) and Chuvieco et al. (2008). To avoid possible confusion with harvested crop land a rough fire perimeter, approximately 1 km outside of the burned area, was manually digitized. Using the 8-day NBR composites as input, the dNBR between each single observation and its five consecutive observations in time was calculated ($dNBR = NBR_t - NBR_{t+i}$ with $i = 1, 2, 3, 4, 5$). When these five dNBR values all exceeded the threshold value of 0.125, the pixel was classified as burned. We have chosen a relatively low threshold to minimize the omission error on low severity pixels. The accuracy of the burned area map was verified using a TM-derived burned area map (Veraverbeke et al., 2010).

For valid control plot estimates, control pixels must correspond to the focal pixel in case the fire had not occurred. Firstly, this implies identical pre-fire characteristics for both control and focal pixels. Secondly, it means similar post-fire environmental conditions. To determine the appropriate control pixel selection criteria, the method of Lhermitte et al. (2010) was calibrated to our dataset based on post-fire similarity, since we wish to estimate how the NBR would have behaved in case of no fire occurrence. In this context, the accuracy of the control pixel selection is assessed by looking at the i) pre- and post-fire similarity of fictively burned pixels and ii) pre-fire similarity of effectively burned pixels. The first approach allows to effectively assess how parameters $c$, the number of control pixels, and $x$, the number of candidate pixels, and $w \times w$, the window size around the focal pixel, affect the post-fire similarity, where $x$ and $w \times w$ can be used interchangeably as they are linearly related by $x = w^2 - 1$. The second approach allows to assess how the spatial context of actual burns affects the similarity when $x$ and $w \times w$ cannot be interchanged.

In the first approach, a similarity analysis was performed to understand how the post-fire similarity is affected by varying numbers of selected control pixels ($c$) and selection windows sizes ($w \times w$). In this context, 500 unburned pixels were randomly selected and a fictive burning date was set for these pixels at the same composite date the real fire event took place. Subsequently, the sensitivity of dissimilarity criterion $D$ to $c$ and $w \times w$ was assessed for each of these pixels by comparing the outcome for varying number of control pixels ($c = 1, 2, \ldots, 15$) and varying window sizes ($3 \times 3$, $5 \times 5, \ldots$, $25 \times 25$). Evaluation consisted of measuring the temporal dissimilarity for the 500 fictively burned sample pixel between $NBR_t^f$ and $NBR_t^x$ one-year pre-fire and one-year post-fire. This allows to determine how well pre-fire similarity is maintained after a fictive burning date and how pre-/post-fire changes in similarity are related to the number of control pixels ($c$) and window size ($w \times w$)/number of candidate pixels ($x$).

Although for isolated burned pixels window size and the number of candidate pixels are linearly related, it is impossible to work with fixed window sizes in the spatial context of actual burns where

burned areas consist of large patches and not all neighboring pixels are candidate pixels. For example, in the first approach eight candidate pixels are found in 3×3-window (nine pixels minus one burned pixel), while for finding eight candidate pixels for a burned pixel located in the middle of a large burn larger window sizes are required. As a result, the distance of the control pixels to their corresponding focal pixel is variable. Therefore, also the second approach was analyzed, where the pre-fire similarity of 500 randomly chosen effectively burned pixels was evaluated taking into account the spatial context of the actual burns. Comparison of the pre-fire similarity of 500 effectively burned and 500 fictively burned pixels then allows verifying how the selection is influenced by the spatial context of the actual burns.

### 3.3. dNBR and optimality

After the derivation of preprocessed TM NBR images, these layers were bi-temporally differenced. This traditional bi-temporal differencing resulted in an IA and EA dNBR, respectively $dNBR_{TM,IA}$ and $dNBR_{TM,EA}$:

$$dNBR_{TM,IA} = NBR_{TM,2006} - NBR_{TM,2007} \quad (3)$$

$$dNBR_{TM,EA} = NBR_{TM,2006} - NBR_{TM,2008}. \quad (4)$$

Additionally, a MODIS dNBR time series was derived after differencing the respective focal ($NBR_t^f$) and control ($NBR_t^c$) images:

$$dNBR_t = NBR_t^c - NBR_t^f. \quad (5)$$

Thus, in contrast with the traditional pre-/post-fire differencing as applied on the TM imagery, the MODIS dNBR was calculated based on focal and control pixels within the same image. For the same post-fire dates as with the TM dNBR images, the MODIS dNBR images were respectively labeled as $dNBR_{MODIS,IA}$ and $dNBR_{MODIS,EA}$.

For evaluating the optimality of the bi-temporal change detection the MIR–NIR bi-spectral space was considered (see Fig. 5). If a spectral index is appropriate to the physical change of interest, in this case fire-induced vegetation depletion, there exists a clear relationship between the change and the direction of the displacement in the bi-spectral feature space (Verstraete & Pinty, 1996). In an ideal scenario a pixel's bi-temporal trajectory is perpendicular to the first bisector of the Cartesian coordinate system. This is illustrated in Fig. 5 for the displacement from unburned (U) to optimally (O) sensed burned.

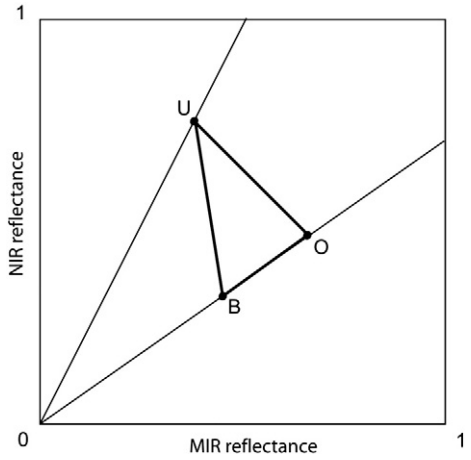


**Fig. 5.** Example pre/post-fire trajectory of a pixel in the MIR–NIR feature space. A pixel displaces from unburned (U) to burned (B). O resembles the position of an optimally sensed burned pixel. The dNBR is sensitive to the displacement |*UO*| and insensitive to the displacement |*OB*|.

Perturbing factors decrease the performance of the index. Then a pixel's displacement can be decomposed in a vector perpendicular to the first bisector and a vector along the post-fire NBR isoline to which the index is insensitive. For example, in Fig. 5, a pixel shifts from unburned (U) to burned (B) after fire. Here, the magnitude of change to which the index is insensitive is equal to the Euclidian distance |*OB*|. Thus the observed displacement vector UB can be decomposed in the sum of the vectors UO and OB, hence, following the expression of Roy et al. (2006) index optimality is defined as:

$$optimality = 1 - \frac{|OB|}{|UB|}. \quad (3)$$

As |*OB*| can never be larger than |*UB*|, the optimality measure varies between zero and one. If the optimality measure equals zero, then the index is completely insensitive to the change of interest. An optimality score of one means that the index performs ideally.

### 3.4. Analysis method

Firstly, the accuracy of the land cover map and the calibration of the control pixel selection procedure are verified. Secondly, the analysis has focused on the correlation between field and TM data for an IA and EA. In addition descriptive dNBR and optimality statistics were compared. To justify the use of MODIS dNBR to explore the temporal dimension the correlation between downsampled TM and corresponding MODIS dNBR imagery is also calculated. Finally, MODIS dNBR and optimality time series for different land cover types are compared. Emphasis has been both on the importance of lag and seasonal timing of an assessment.

## 4. Results

### 4.1. MODIS pre-fire land cover map

Fig. 6 displays the pre-fire land cover map derived based on the time series similarity concept. Shrub land was the most prevailing

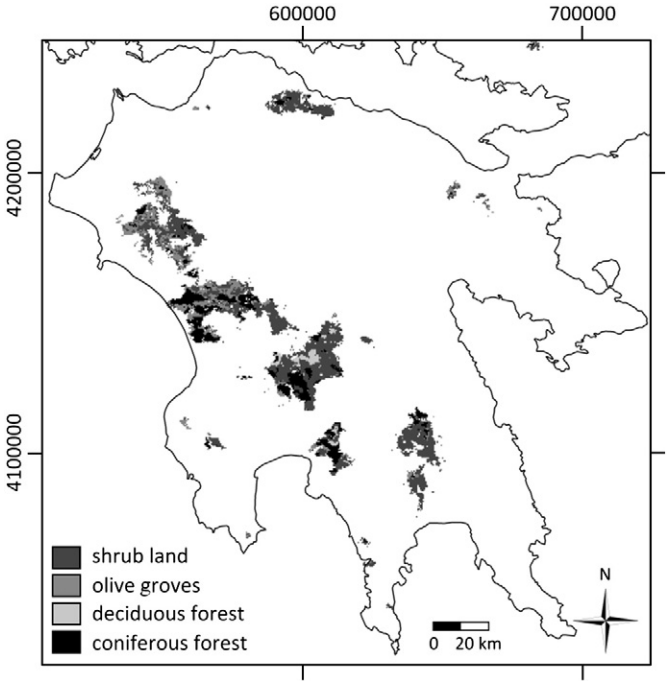


**Fig. 6.** Pre-fire land cover map obtained after performing a maximum likelihood classification on a MODIS NBR time series of the pre-fire year 2006 (temporal profiles of training samples are given in Fig. 4).

land cover type. 100,372 ha (56.65% of the burned area) were classified as shrub land. The class coniferous forest covered 37,096 ha (20.95% of the burned area) which was only slightly more than the olive groves class (34,555 ha, 19.50% of the burned area). A minority of the pixels were classified as deciduous forest (624 ha, 2.90%). The error matrix of the land cover map is tabulated in Table 2. The overall accuracy of the classification equalled 73% and a Kappa coefficient of 0.60 was obtained. As the phenology of deciduous forest contrasts with those of evergreen land cover classes (see Fig. 4), this class obtained high producer's and user's accuracies of respectively 81% and 93%. The evergreen land cover classes revealed a higher time series similarity. As a result these cover classes were prone to higher omission and commission errors. These errors remained, however, acceptable. The classification of shrub land resulted in both a producer's and user's accuracy of 75%. The producer's accuracy of coniferous forest equalled 72%, which was slightly lower than its user's accuracy of 76%. Finally, the accuracy of olive groves class was the lowest (producer's and user's accuracy of respectively 64% and 47%).

### 4.2. MODIS control pixel selection

TM imagery was used to validate the MODIS burned area map. The TM-derived burned area map was derived after applying a two-phase $dNBR_{TM,IA}$ threshold algorithm that was validated using field reference data resulting in a detection probability of 80% and a probability of false alarm of 5% (Veraverbeke et al., 2010). MODIS burned area statistics were extracted in windows of 10 by 10 km. These statistics were regressed against their TM equivalents, in which the TM data acted as independent variable and the MODIS data as dependent variable. The resulting regression slope and intercept equaled respectively 1.31 and −27.97. The MODIS-derived burned area map correlated fairly well with the TM-based map (coefficient of determination $R^2 = 0.98$, $p < 0.001$), although a consistent overestimation relative to the TM data was perceived as indicated by the regression slope of 1.31.

Fig. 7A reflects the *D* in function of varying number of control pixels and window size for a pre-fire year. It shows the median temporal similarity of the 500 unburned sample pixels. The median is used instead of the mean as it is more robust in the presence of outlier values. Two main effects are observed in the figure. Firstly, the number of control pixels chosen influenced the dissimilarity measure due to an averaging effect. The strength of this averaging effect was dependent on window size: the averaging effect became more important for larger window sizes. Secondly, there was a consistently decreasing trend in pre-fire *D* when window size enlarged. This feature appeared regardless of the number of control pixels chosen. The latter finding contrasts with what is visible in Fig. 7B, which represents the post-fire *D* in function of varying number of control pixels and window size. Here, one can see a consistently increasing trend in *D* as window size became larger. As a result, differences between pre- and post-fire similarity enlarged in proportion with window size. This effect originates from the possible selection of distant pixels that have higher probability of showing different post-fire environmental conditions in larger windows (Lhermitte et al., 2010). Fig. 7C displays pre-fire similarity of the 500 burned sample pixels. The *x*-axis is expressed in terms of the number of candidate pixels instead of window size, because the spatial context of actual burns makes windows size variable. The abscissas of Fig. 7C correspond with the number of candidate pixels present in the windows mentioned in Fig. 7A–B. Similar to what is observed in Fig. 7A, one can see both an averaging effect and consistently decreasing *D* for an increasing number of candidate pixels. The main difference between Fig. 7A and C is that overall, dissimilarity *D* is higher in Fig. 7C.

In these figures one can infer that (i) the post-fire similarity is higher for small windows (less candidate control pixels) than for larger windows (more candidate control pixels), (ii) averaging of more than three pixels results in a higher temporal similarity than using less than four control pixels, (iii) the trends in pre-fire similarity (averaging effect and increasing similarity for increasing number of candidate pixels) are the same as for the fictive and effective burned pixels. These findings combined with the consideration that it is impossible to work with fixed window due to the spatial context of actual burns (e.g., to retrieve eight candidate pixels relatively small windows are necessary near the contours of a burn, whereas larger window sizes are required for burned pixels in the middle of a large fire scar) govern the final decision criterion to determine control pixels. Based on these considerations the control pixel selection criterion was defined as taking the average of the four most similar pixels out of eight candidate pixels, which corroborates with the findings of Lhermitte et al. (2010). This criterion combines the need for proximate pixels and beneficial averaging.

### 4.3. Relationship between field, TM and MODIS data

Table 3 lists some descriptive statistics as derived from the $dNBR_{TM,IA}$, $dNBR_{TM,EA}$ $dNBR_{MODIS,IA}$ and $dNBR_{MODIS,EA}$ layers. Mean dNBR was clearly higher for an IA than for an EA, for both TM and MODIS assessments (0.56 vs. 0.29 for TM, 0.44 vs. 0.21 for MODIS). The same was true for mean optimality (0.65 vs. 0.47 for TM, 0.68 vs. 0.50 for MODIS). The standard deviation (sd) of the dNBR sd was also higher in IA than in EA (0.29 vs. 0.19 for TM, 0.19 vs. 0.14 for MODIS). This contrasts with the lower optimality sd of IAs compared to EAs (0.25 vs. 0.29 for TM, 0.24 vs 0.30 for MODIS). Mean and sd dNBR were higher for TM assessment than for MODIS assessments. Mean optimality, however, was slightly higher for MODIS assessments, while inter-sensor differences in sd optimality were minor.

Table 4 summarizes the regression results between field, TM and MODIS data. All results were based on 150 observations, corresponding to the GeoCBI locations. Comparison of the $R^2$ statistics shows that the GeoCBI–$dNBR_{TM}$ relationship proved to be the strongest for the IA scheme. This relationship yielded a moderate–high $R^2 = 0.72$ for a linear fitting model. This is higher than the GeoCBI–$dNBR_{TM,EA}$ correlation which had an $R^2 = 0.56$. After downsampling the TM pixels to the MODIS resolution, linear regressions were also performed between the downsampled TM and the MODIS dNBR. These regressions resulted in a moderate correlations of $R^2 = 0.59$ for the IA and $R^2 = 0.45$ for the EA scheme.

### 4.4. Post-fire MODIS dNBR and optimality time series per land cover type

Figs. 8–11 show the temporal profiles of mean NBR (±sd) of control and focal pixels (A), mean dNBR (±sd) (B) and mean optimality (±sd) (C) of respectively shrub land, olive groves, coniferous forest and deciduous forest. The control pixels' mean NBR of the evergreen species (shrubs, olives and conifers) showed little seasonal variations, which accords with and Fig. 4 and statements in Section 3.1. In contrast, the temporal development of the mean NBR of deciduous forest was dominated by a clear summer maximum and winter minimum. These dissimilarities in seasonality between evergreen and deciduous land

**Table 2**
Error matrix of the pre-fire land cover map (accuracy verified based on 150 reference points). The overall accuracy (0.73) and the Kappa coefficient (0.60) are indicated in bold.

| | | Reference data | | | | User's accuracy |
|---|---|---|---|---|---|---|
| | | S | O | D | C | |
| Classified data | S | 47 | 5 | 1 | 10 | 0.75 |
| | O | 3 | 9 | 1 | 6 | 0.47 |
| | D | 1 | 0 | 13 | 0 | 0.93 |
| | C | 12 | 0 | 1 | 41 | 0.76 |
| Producer's accuracy | | 0.75 | 0.64 | 0.81 | 0.72 | **0.73** |
| | | | | | Kappa | **0.60** |

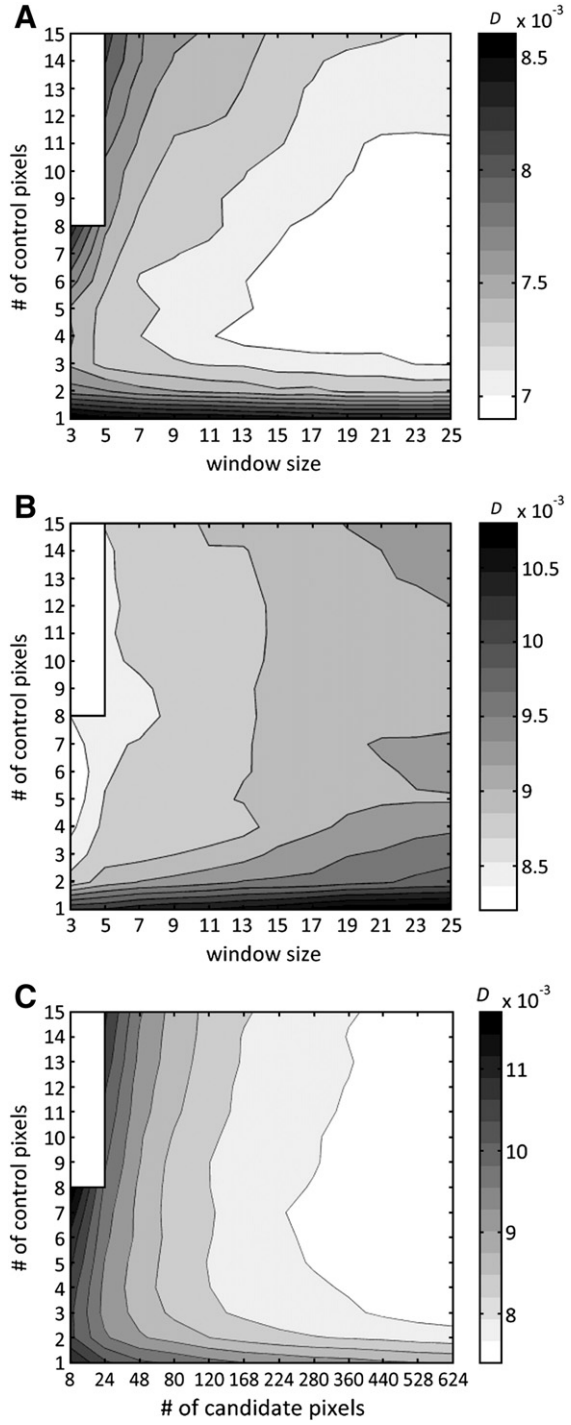


**Fig. 7.** Median dissimilarity *D* of the 500 fictively burned sample pixels in function of varying number of control pixels and window size for (A) a pre-fire year, for (B) a post-fire year (for the post-fire year, the same control pixels setting as in the pre-fire year is preserved) and median dissimilarity *D* of the 500 burned sample pixels in function of varying number of control pixels and candidate pixels for a pre-fire year (C). The grayscale reflects the temporal similarity, while the white areas in the upper-left corner represent impossible combinations (number of control pixels>8, for 3×3 window size).

cover impact the dNBR and its optimality. Recovery processes were prevalent for the evergreens (Figs. 8–10). As a result mean dNBR (and sd) and mean optimality progressively decreased as time elapsed. Shrub land (Fig. 8) and olive groves (Fig. 9) revealed very similar temporal patterns. Recovery peaked during early spring (April–May), which is characteristic for xerophytic species in the Mediterranean. This caused a clear drop in both mean dNBR and mean optimality. The absolute magnitude of change was slightly higher for coniferous forest (mean dNBR up to 0.60) than for shrubs and olive groves (mean dNBR up to 0.50). Immediately post-fire mean optimality was higher than 0.70 for the evergreen cover types. However, the optimality statistic clearly dropped after two months post-fire. Conversed to the evergreens, inter-annual variations are important in deciduous forest. Immediately post-fire the difference between the control and focal pixels' mean NBR values is large. This difference diminished as time elapsed due to two main processes. Firstly, leaf-fall caused the control pixels' index to drop. Secondly, regeneration processes produced an increase of the focal pixels' NBR values. By the start of the next growing season, however, the difference between control and focal pixels became again more explicit. The abovementioned processes also provoked a clear seasonality in both temporal mean dNBR (Fig. 11B) and optimality (Fig. 11C). Initially mean dNBR values were (up to 0.60) high with corresponding high optimality scores (up to 0.70). During winter mean dNBR values were very low (minimum of 0.10) was reached, and this also resulted in low mean optimality scores below 0.40. By the onset of next growing season both mean dNBR and optimality recovered.

**Table 3**
Descriptive dNBR and optimality statistics of the TM and MODIS IA and EA.

| | TM | | MODIS | |
|---|---|---|---|---|
| | IA | EA | IA | EA |
| Mean dNBR (±sd) | 0.56 (0.29) | 0.29 (0.19) | 0.44 (0.19) | 0.21 (0.14) |
| Mean optimality (±sd) | 0.65 (0.25) | 0.47 (0.29) | 0.68 (0.24) | 0.50 (0.30) |

## 5. Discussion

### 5.1. Control pixel selection

The strength of the control pixel selection procedure is that the post-fire temporal behaviour of the NBR, dNBR and optimality is estimated on a per-pixel-basis and free of image-to-image normalization constraints. The method relies on pre-fire time series similarity between focal burned pixels and unburned control pixels where the main driver of the control pixel selection setting is post-fire similarity, since we wish to estimate how the NBR would have behaved in case of no fire occurrence. In this context, the control pixel selection settings can only be assessed by looking at the post-fire similarity of fictively burned pixels in Fig. 7B. In this figure, one can see two effects: i) the similarity is clearly higher for small windows than for larger windows and ii) averaging of more than three pixels results in a higher temporal similarity than using less than four control pixels. The former effect arises from the possible selection of distant pixels with different post-fire meteorological conditions for larger window sizes (Lhermitte et al., 2010). Our recommendation to select control pixels in close vicinity to the burned areas corroborates with findings of Li et al. (2008) and fulfils the general rule that terrain features in a close vicinity are more likely to be similar than distant features (Tobler, 1970). The latter effect arises from beneficial averaging, which is rather remarkable as one would expect that the use of only the most similar pixel would give the best result. However, noise reduces the similarity between the most similar control and the focal pixel. Even

**Table 4**
Linear regression results between on the one hand GeoCBI field data and $dNBR_{TM}$, on the other between downsampled $dNBR_{TM}$ and $dNBR_{MODIS}$ in both IA and EA schemes ($n=150$, $p<0.001$).

| Model form | a (±sd) | b (±sd) | $R^2$ |
|---|---|---|---|
| $GeoCBI = a \times dNBR_{TM,IA} + b$ | 0.649 (0.033) | 1.455 (0.019) | 0.72 |
| $GeoCBI = a \times dNBR_{TM,EA} + b$ | 0.767 (0.056) | 1.508 (0.018) | 0.56 |
| $dNBR_{TM,IA} = a \times dNBR_{MODIS,IA} + b$ | 0.067 (0.037) | 0.804 (0.069) | 0.59 |
| $dNBR_{TM,EA} = a \times dNBR_{MODIS,EA} + b$ | 0.035 (0.022) | 0.730 (0.082) | 0.45 |

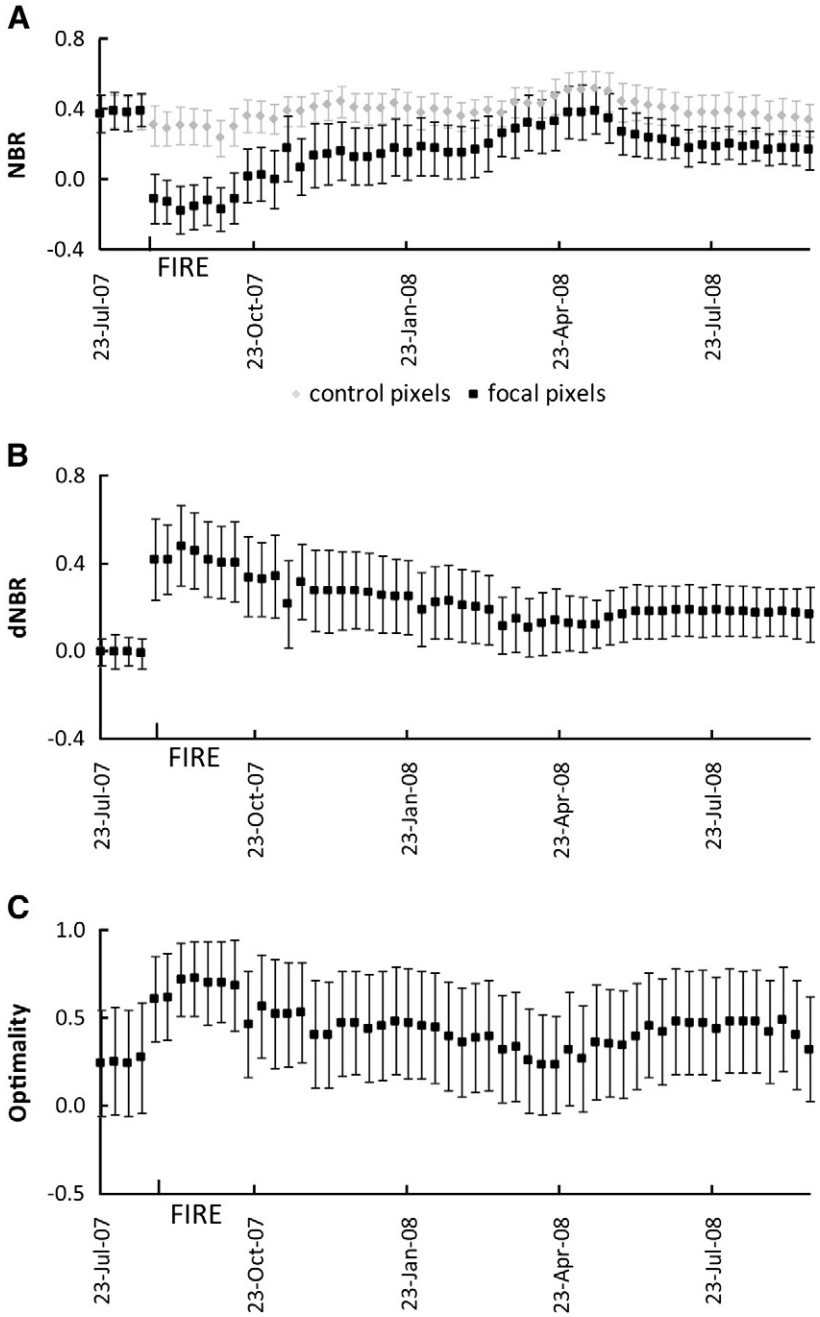


**Fig. 8.** Time series of (A) mean NBR of control and focal pixels, (B) mean dNBR and (C) mean optimality (C) shrub land pixels before the fire event. The vertical bars indicate the sd.

after preprocessing, a certain amount of random noise remains present in the data set. Averaging the two or more most similar pixels causes a more temporally stable signal because random noise is averaged out resulting in a higher temporal similarity with the focal pixel (Lhermitte et al., 2010). This beneficial averaging effect is, however, finite as at a certain point non-similar pixels will also be included in the averaging process, which will deteriorate the similarity.

Although post-fire similarity determines the settings of the procedure, the selection of the pixels itself needs to be executed on pre-fire time series. In both Fig. 7A and C similarity increases for larger window sizes. This effect, however, is not relevant as the spatial heterogeneity in for example meteorology has a large inter-annual variability. This is why post-fire similarity in Fig. 7B, although based on the same settings as pre-fire similarity in Fig. 7A, decreases with increasing window size. Combination of both the favorable post-fire similarity in small windows and the existence of a beneficial averaging effect govern the final decision to select four control pixels out of eight candidate pixels.

The calibration experiment on the 500 fictively burned pixels does not mimic the spatial context of the actual burns. The calibration experiment is based on isolated pixels, while in reality burned areas consist of several large patches. For burned pixels, who are partly surrounded with other burned pixels, larger windows than a $3\times3$-window are required to retrieve eight control pixels. This makes the window size dependent on the position of the burned pixel in its patch. For pixels close to the fire perimeter window size will be relatively small, whereas for pixels in the middle of a large burn window sizes need to larger. As nearby pixels have a higher probability to be similar than distant pixels (Li et al., 2008; Tobler, 1970), the spatial context of the actual burns results in a lower similarity than what was observed in the calibration experiment based on fictively isolated pixels (Fig. 7A and C). Pre-fire similarity retrieved from the 500 burned pixels in

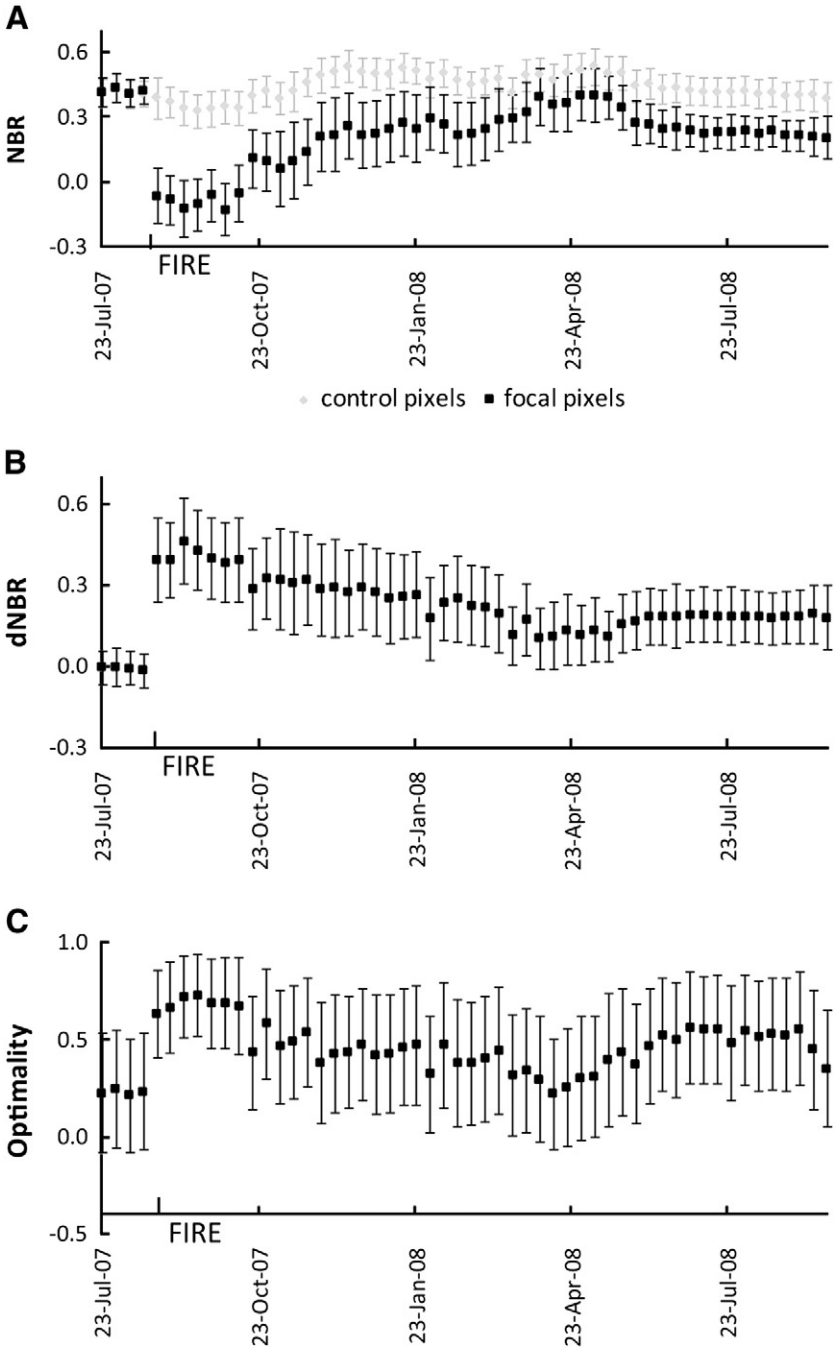


**Fig. 9.** Time series of (A) mean NBR of control and focal pixels, (B) mean dNBR and (C) mean optimality (C) olive groves pixels before the fire event. The vertical bars indicate the sd.

function of the number of candidate pixels and the number of control pixels is, however, characterized by the same trends as observed in the calibration experiment. One can expect that if it would be possible to calculate post-fire similarity on the actual burns, the same trends, probably with a slightly lower overall similarity, of the calibration experiment (Fig. 7B) would manifest.

Despite of the merits of the control pixel selection procedure as presented in this paper two constraints remain. Firstly, due to the necessity to search in larger windows for pixels in the middle of the burn the performance of the procedure is likely to be better near the contours of the burn perimeter. On the one hand this is inevitable as the potentially most similar neighbor pixels are also burned. On the other hand one could argue that this phenomenon incites to make the control pixel selection settings dependent on the distance to the fire perimeter. The procedure is also affected by a second constraint, i.e. the heterogeneity of the unburned landscape matrix. It is trivial that the procedure will be more optimal in highly homogeneous landscapes, even for large search windows. In contrast, in highly heterogeneous mixtures of different land cover types the procedure will potentially fail to retrieve similar pixels for small window sizes. It is a hard task to uncouple and quantify the effects of both constraints. Solutions to this have the potential to further improve the selection procedure.

### 5.2. Lag timing

Regression results between $dNBR_{TM}$ and field data were clearly influenced by the lag timing of the assessment (Table 4). Although this corroborates with the findings of Zhu et al. (2006) and Allen and Sorbel (2008), it contrasts with Fernandez-Manso et al. (2009) who

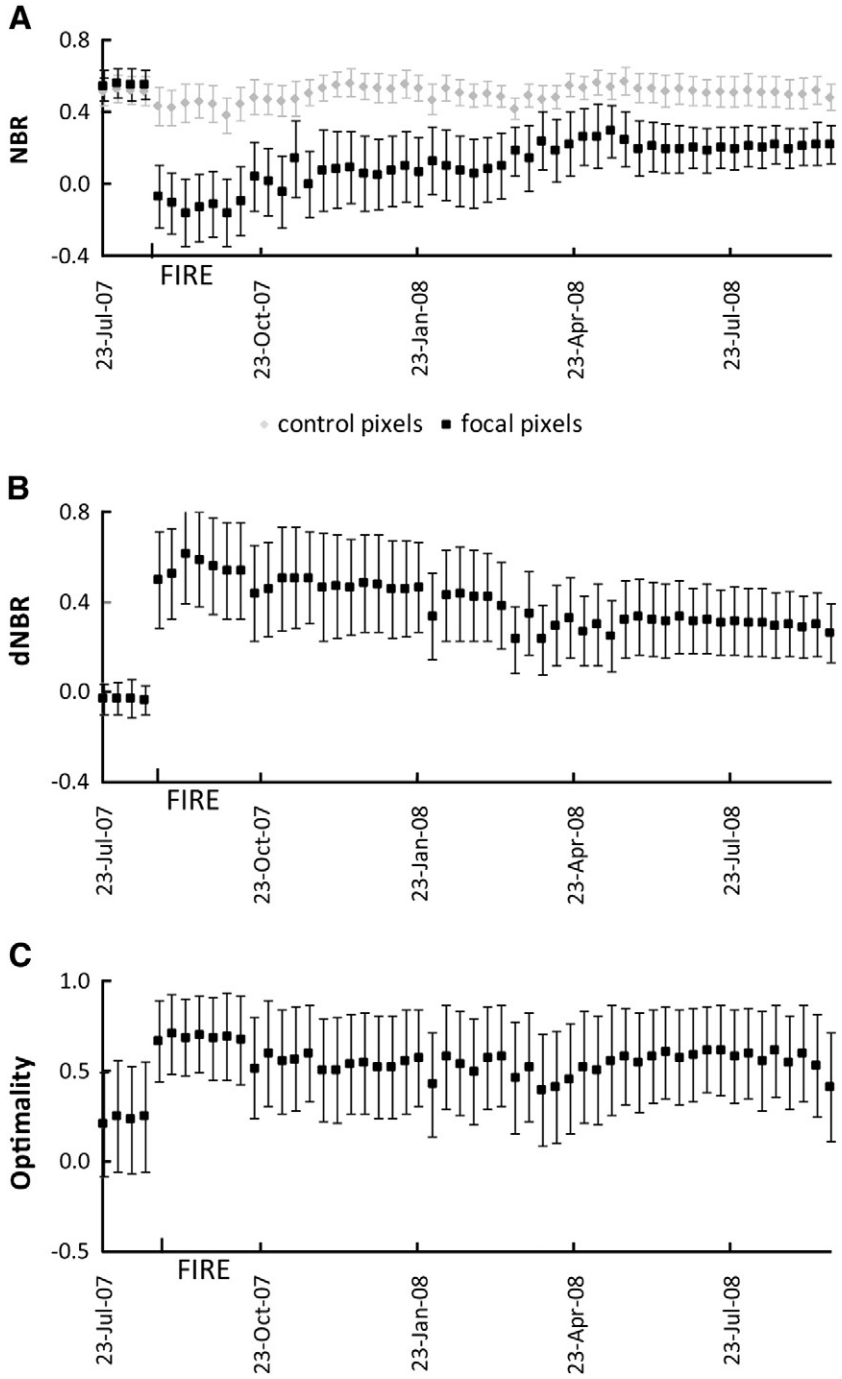


**Fig. 10.** Time series of (A) mean NBR of control and focal pixels, (B) mean dNBR and (C) mean optimality (C) coniferous forest pixels before the fire event. The vertical bars indicate the sd.

state that the difference between an IA and EA does not significantly influences the remotely sensed magnitude of change. In our study the correlation between field and TM data was better for the IA ($R^2 = 0.72$) than for the EA ($R^2 = 0.56$), which is opposite to the observations of Zhu et al. (2006). Following these authors, however, the poorer regression fits for IA are merely attributed to unfavorable remote sensing conditions (low sun angles, smoke, bad weather, snow and clouds), and not necessarily to differences in lag timing. Additionally, Allen and Sorbel (2008) found that initial and extended assessments produced significantly different information with regards to burn severity for tundra vegetation, while the timing of the assessment had no effect for black spruce forest, which was attributed to the rapid tundra recovery. As in our study, this demonstrates that in quickly recovering ecosystems first-order effects such as vegetation consumption, scorching and charring are mitigated by resprouters (Key, 2006; Lhermitte et al., submitted for publication). This is also visible when the magnitude of change and the within-burn variation between IA and EA schemes are compared (Table 3). For both TM and MODIS assessment, mean dNBR almost halved whereas sd dNBR was also clearly lower for the EA. This reduction in variability highly impacts the suitability of the dNBR for burn severity mapping. The within-burn variation of the MODIS assessments was lower than with TM assessment as a result of the 500 m resolution compared to the 30 m resolution of the TM sensor. Correlations between downsampled $dNBR_{TM}$ and corresponding $dNBR_{MODIS}$ were moderate, which justifies the use of MODIS NBR time series as a way of exploring the temporal

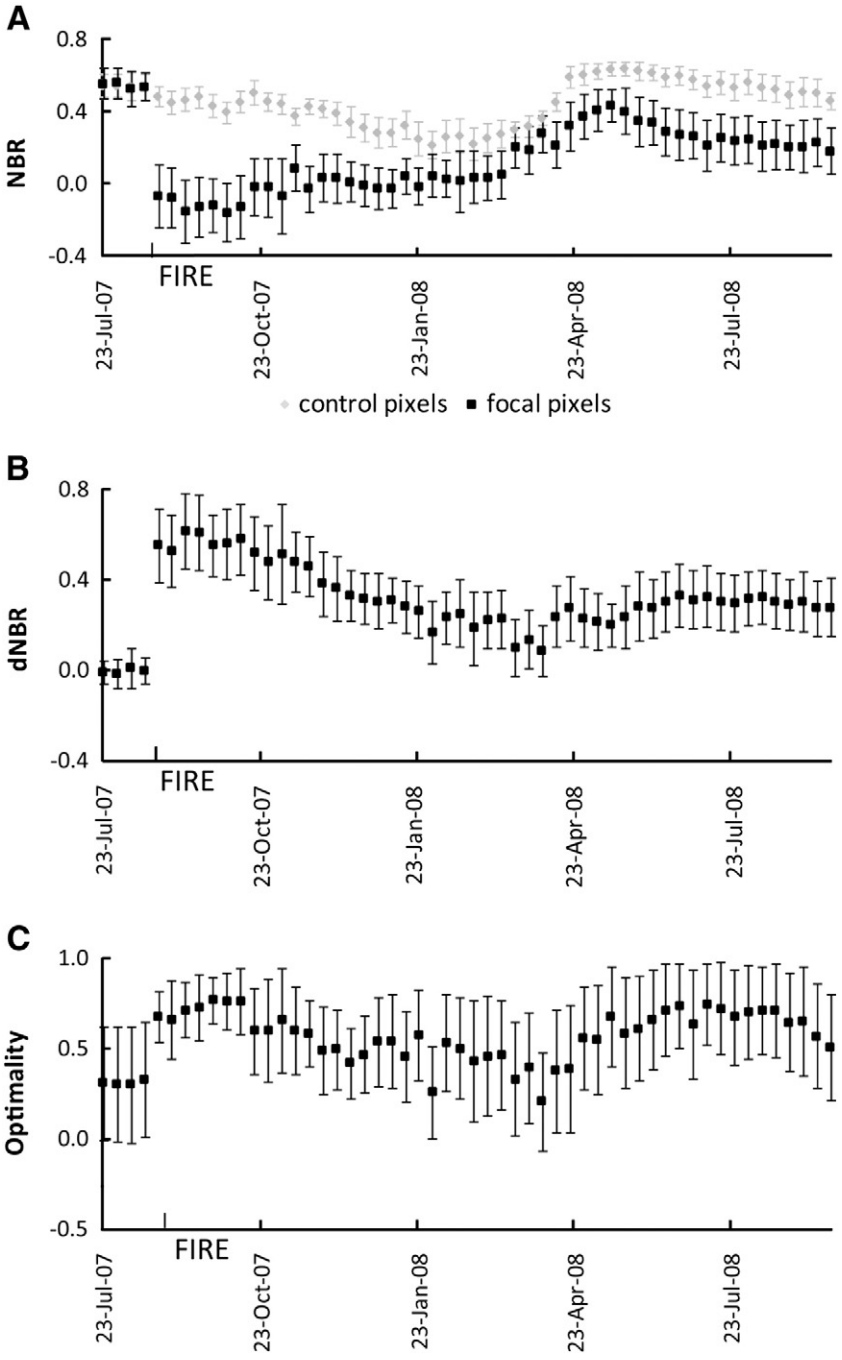


**Fig. 11.** Time series of (A) mean NBR of control and focal pixels, (B) mean dNBR and (C) mean optimality (C) deciduous forest pixels before the fire event. The vertical bars indicate the sd.

dimension of remote sensing of post-fire effects. We are aware that by doing so spatial heterogeneity is sacrificed to some degree (Key, 2006). Differences between downsampled $dNBR_{TM}$ and $dNBR_{MODIS}$ can be attributed to the use of single-data imagery vs. 8-day composites, discrepancies between traditional bi-temporal differencing and control pixel selection procedure, differences in preprocessing (e.g. modified c-correction vs. no topographic correction), MODIS's geolocation error (Wolfe et al., 1998), etc.

Previous studies have analyzed the dNBR's optimality for assessing fire/burn severity, most of them based on Landsat imagery (Escuin et al., 2008; Murphy et al., 2008; Roy et al., 2006; Veraverbeke et al., 2010, in press—b). This resulted in a moderate mean optimality of 0.49 (Escuin et al., 2008) and between 0.26 and 0.80 for six burns in Alaska, United States (Murphy et al., 2008). Clearly lower mean dNBR optimality scores (0.10) were reported by Roy et al. (2006) for African savannah burns. These authors also report low dNBR optimality values for MODIS sensed fires in other ecosystems (Russia, Australia, South America). These results suggest that the dNBR is suboptimal for assessing fire/burn severity. The poor optimality results obtained by Roy et al. (2006) can partly be explained by the fact that the authors also included unburned pixels in their analysis. Unaffected pixels are generally associated with low optimality scores since a pixel's shift in the bi-spectral space is then only caused by noise (Escuin et al., 2008). Veraverbeke et al. (2010) revealed the influence of illumination effects on dNBR optimality after which they proposed a topographic correction that significantly improved the reliability of the assessment. Despite of the merits of these studies, none of them researched the time-dependency of the optimality statistic. The descriptive

optimality statistics (Table 3) reveal the influence of assessment timing on the performance of the dNBR. The IAs had clearly higher optimality scores than EAs, e.g. for the TM assessment respectively 0.65 (±0.25) and 0.47 (±0.29). Mean optimality values achieved maximum values the first two months post-fire (Figs. 8C, 9C, 10C and 11C). At the moment of maximum optimality, the sd of the optimality statistic reached its minimum elucidating its stability. Based on the optimality statistic one can indicate the first two months post-fire as the best period to assess post-fire effects, at least in this study. This period also corresponds with the highest magnitude of change in dNBR (Figs. 8B, 9C, 10C and 11C) and with a relatively high degree in variation. Results based on our TM data slightly differ from previously published outcomes based on the same data (Veraverbeke, in press—a,b, 2010), mainly because of some minor changes in satellite preprocessing and the exclusion of 10 unburned field plots.

### 5.3. Seasonal timing

An important recommendation when doing bi-temporal change detection is that the image couple should approximate as closely as possible the anniversary date acquisition scheme (Coppin et al., 2004). This diminishes illumination differences and phenological dissimilarities. Because of Landsat's infrequent acquisition of cloud-free imagery (Ju & Roy, 2008) bi-temporal acquisition schemes potentially diverge from the ideal anniversary data scheme. This causes problems as external influences (e.g. illumination conditions, plant phenology) then distort the evaluation of post-fire effects (Veraverbeke et al., 2010; Verbyla et al., 2008). Verbyla et al. (2008) demonstrated false trends in dNBR as a consequence of combined seasonal and topographic effects, while Veraverbeke et al. (2010) recommended performing topographic corrections, even for ratio-based analysis, as the general assumption that ratioing reflectance data removes shade effects does not necessarily hold true. These issues are merely concerned with traditional image-to-image normalization constraints (Song & Woodcock, 2003). The application of the control pixel selection procedure, however, makes the MODIS dNBR time series free of these limitations (Diaz-Delgado & Pons, 2001; Lhermitte et al., 2010). Comparison of Figs. 8–11 discloses some important findings. Firstly, only slight differences in assessment timing can result in distinct index values. On the one side this results from recovery processes (see Section 5.2), but on the other side seasonal changes in both control and focal pixels are also important. In our study area for example, the herbaceous resprouters show a clear rise in NBR values during spring, which is a period of favorable hydro-thermic conditions (Fig. 3, Specht, 1981; Maselli, 2004). As a consequence corresponding dNBR and optimality values drop during this period. In the one-year post-fire summer productivity of regenerating plants diminishes again which results in a generally better index performance. Secondly, phenological patterns can greatly vary between different land cover types (Lhermitte et al., 2008; Reed et al., 1994; Viovy, 2000). Fig. 11A, which displays the NBR time series of deciduous forest, contrasts with those of Figs. 8A, 9A and 10A. This is because the evergreen land cover types (shrub land, coniferous forest and olive groves) typically have a productivity that remains more or less stable throughout the year while deciduous forest is characterized by a clear winter minimum and summer maximum. As a consequence, while the seasonal timing of an assessment produces only small differences for evergreen species, it is crucial for deciduous forest. When this consideration is forgotten, an assessment in deciduous land cover types risks to measure plant phenology (e.g. leaf senescence) instead of the fire effects, which can falsify fire/burn severity estimations. Similar findings were achieved by Lhermitte et al. (submitted for publication). In this study, conducted in a savanna environment, intra-annual changes in index values were dominated by the grass layer. The assessment was therefore strongly influenced by its seasonal timing. Summarized for our study area, a Mediterranean-type ecosystem (MTE) with a mixture of land covers, the summer period is preferential for fire/burn severity assessments. This timing reduces the occurrence of phenological discrepancies between different land covers.

### 5.4. Implications for Landsat dNBR fire/burn severity assessments

Increasingly, fire researchers become interested in detecting trends in fire/burn severity (Eidenshink et al., 2007; Miller et al., 2008; Verbyla et al., 2008). To fulfill this duty it is of paramount importance that assessment are comparable across space and time. The relative version of the dNBR (RdNBR), which is defined as the dNBR divided by the square root of the pre-fire NBR, hypothetically allows a better comparison among different land cover types, especially in heterogeneous landscapes. This was made clear for fires in conifer dominated vegetation types in California, USA (Miller et al., 2009). Whereas the hypothetical advantage of the relative index to account for spatial heterogeneity has an intuitive appeal, the index does not handle temporal differences which may be present among different assessments. In this respect our study demonstrates that only small differences in Landsat acquisition timing can result in significantly other dNBR and optimality values. This results from both lag and seasonal constraints. The latter requires a profound knowledge of the covers affected by the fire and their phenological development, especially when the land covers reveal dissimilar intra-annual patterns. Lag timing is important as vegetation regrowth mitigates first-order fire effects (Key, 2006; Zhu et al., 2006). This affects the magnitude of change, the variability and the index performance of what is actually measured. For our Mediterranean study area, correlation with field data, dNBR variability and optimality were clearly higher for an IA than for an EA. Additionally, optimality was the highest the first two months post-fire. In other ecosystems, however, EAs trended better with field data (Zhu et al., 2006). The NBR was originally developed for the use in temperate and boreal ecosystems (Key & Benson, 2005; Eidenshink et al., 2007; French et al., 2008 among them), which are characterized by a relative slow recovery (Cuevas-Gonzalez et al., 2009). For these ecoregions it is plausible that lag timing not significantly alters the information content of an assessment. The lag timing of assessment in quickly recovering ecosystems, however, determines how post-fire effects are measured. Fire severity is estimated with better contrast and higher reliability, while first-order effects are obscured by regeneration processes when assessing burn severity. This incites caution for the use of the NBR for assessing burn severity in quickly recovering ecosystems.

Of course bi-temporal Landsat assessments are limited by the infrequent image availability (Ju & Roy, 2008). Moreover, whether or not ecosystem responses are included in the study makes an important ecological difference and depends on the goals of the project. Within these limitations, however, one should be aware of the temporal dimension of the remote sensing of post-fire effects. In this context, we urge for a transparent and consistent use of terminology as presented in Fig. 1. In this we follow Lentile et al. (2006) who suggested a substantial difference between the terms fire and burn severity. From a remote sensing point of view, our results support this important difference and question the recommendation of Keeley (2009) to treat both terms as mutually interchangeable. Both terms assess the direct fire impact but only burn severity includes ecosystem responses.

## 6. Conclusions

The goal of this paper was to elaborate on the temporal dimension of dNBR fire/burn severity studies. In this context fire severity was defined as the degree of environmental change caused by fire as measured immediately post-fire, whereas burn severity combines the direct fire impact and ecosystem responses. The study made use of

field, TM and MODIS data. An IA and EA were calculated based on pre-/post-fire differenced TM imagery. Additionally a MODIS dNBR time series was generated by using the control pixel selection procedure. This procedure uses the time series similarity concept to assign a unique control pixel to each burned pixel, which allows differencing within the same image. The large 2007 Peloponnese (Greece) wildfires were chosen as case study.

Results showed a clearly better correlation with field data for the IA than for the EA. In addition, the magnitude, variability and optimality of the dNBR were better early post-fire than one-year post-fire. Moreover, the highest index optimality was reached the first two months post-fire. In quickly recovering ecosystems, thus, regeneration processes mitigate first-order fire effects, which can obscure burn severity estimations. This demonstrates the influence of the lag timing of an assessment. Results also revealed that land cover specific intra-annual variations influence to a high degree dNBR and optimality outcomes. For example in the Mediterranean, favorable hydro-thermic conditions during spring enhance the productivity of herbaceous species in the burned areas. This, however, makes the dNBR unsuitable to measure fire effects during this period. As such, an appropriate seasonal timing of an assessment is of paramount importance to minimize false trends. Although these findings are specific to our case study, similar temporal constraints can be expected in other ecoregions. Our findings urge, within the limitations of available Landsat imagery, for awareness of the temporal dimension in the remote sensing of post-fire effects. In this context, we also propose clarification in associated terminology.

## Acknowledgements

The study was financed by the Ghent University special research funds (BOF: Bijzonder Onderzoeksfonds). The authors would like to thank the anonymous reviewers for their constructive remarks.

## References

Allen, J., & Sorbel, B. (2008). Assessing the differenced Normalized Burn Ratio's ability to map burn severity in the boreal forest and tundra ecosystems of Alaska's national parks. *International Journal of Wildland Fire*, *17*, 463−475.

Barbosa, P., Gregoire, J., & Pereira, J. (1999). An algorithm for extracting burned areas from time series of AVHRR GAC data applied at a continental scale. *Remote Sensing of Environment*, *69*, 253−263.

Barbosa, M., Pereira, J., & Gregoire, J. (1998). Compositing criteria for burned area assessment using multitemporal low resolution satellite data. *Remote Sensing of Environment*, *65*, 38−49.

Bisson, M., Fornaciai, A., Coli, A., Mazzarini, F., & Pareschi, M. (2008). The Vegetation Resilience After Fire (VRAF) index: Development, implementation and an illustration from central Italy. *International Journal of Applied Earth Observation and Geoinformation*, *10*, 312−329.

Brewer, K., Winne, C., Redmond, R., Opitz, D., & Mangrich, M. (2005). Classifying and mapping wildfire severity: A comparison of methods. *Photogrammetric Engineering & Remote Sensing*, *71*, 1311−1320.

Capitaino, R., & Carcaillet, C. (2008). Post-fire Mediterranean vegetation dynamics and diversity: A discussion of succession models. *Forest Ecology and Management*, *255*, 431−439.

Chafer, C. (2008). A comparison of fire severity measures: An Australian example and implications for predicting major areas of soil erosion. *Catena*, *74*, 235−245.

Chafer, C., Noonan, M., & Macnaught, E. (2004). The post-fire measurement of fire severity and intensity in the Christmas 2001 Sydney wildfires. *International Journal of Wildland Fire*, *13*, 227−240.

Chander, G., Markham, L., & Barsi, J. (2007). Revised Landsat-5 Thematic Mapper radiometric calibration. *IEEE Geoscience and Remote Sensing Letters*, *4*, 490−494.

Chavez, P. (1996). Image-based atmospheric corrections—Revisited and improved. *Photogrammetric Engineering & Remote Sensing*, *6*, 1025−1036.

Chuvieco, E., Englefield, P., Trishchenko, A., & Luo, Y. (2008). Generation of long time series of burn area maps of the boreal forest from NOAA-AVHRR composite data. *Remote Sensing of Environment*, *112*, 2381−2396.

Chuvieco, E., Ventura, G., Martin, P., & Gomez, I. (2005). Assessment of multitemporal compositing techniques of MODIS and AVHRR images for burned land mapping. *Remote Sensing of Environment*, *94*, 450−462.

Cihlar, J. (1996). Identification of contaminated pixels in AVHRR composite images for studies of land biosphere. *Remote Sensing of Environment*, *56*, 149−163.

Cocke, A., Fule, P., & Crouse, J. (2005). Comparison of burn severity assessments using differenced normalized burn ratio and ground data. *International Journal of Wildland Fire*, *14*, 189−198.

Coppin, P., Jonckheere, I., Nackaerts, K., & Muys, B. (2004). Digital change detection techniques in ecosystem monitoring: A review. *International Journal of Remote Sensing*, *25*, 1565−1595.

Cuevas-Gonzalez, M., Gerard, F., Baltzer, H., & Riano, D. (2009). Analysing forest recovery after wildfire disturbance in boreal Siberia using remotely sensed vegetation indices. *Global Change Biology*, *15*, 561−577.

De Santis, A., & Chuvieco, E. (2009). GeoCBI: A modified version of the Composite Burn Index for the initial assessment of the short-term burn severity from remotely sensed data. *Remote Sensing of Environment*, *113*, 554−562.

Diaz-Delgado, R., Lloret, F., & Pons, X. (2003). Influence of fire severity on plant regeneration by means of remote sensing. *International Journal of Remote Sensing*, *24*, 1751−1763.

Diaz-Delgado, R., & Pons, X. (2001). Spatial patterns of forest fires in Catalonia (NE of Spain) along the period 1975–1995: Analysis of vegetation recovery after fire. *Forest Ecology and Management*, *147*, 67−74.

Dwyer, E., Perreira, J., Grégoire, J., & DaCamara, C. (1999). Characterization of the spatio-temporal patterns of global fire activity using satellite imagery for the period April 1992 to March 1993. *Journal of Biogeography*, *27*, 57−69.

Eidenshink, J., Schwind, B., Brewer, K., Zhu, Z., Quayle, B., & Howard, S. (2007). A project for monitoring trends in burn severity. *Fire Ecology*, *3*, 3−21.

Epting, J., & Verbyla, D. (2005). Landscape-level interactions of prefire vegetation, burn severity, and postfire vegetation over a 16-year period in interior Alaska. *Canadian Journal of Forest Research*, *35*, 1367−1377.

Epting, J., Verbyla, D., & Sorbel, B. (2005). Evaluation of remotely sensed indices for assessing burn severity in interior Alaska using Landsat TM and ETM+. *Remote Sensing of Environment*, *96*, 328−339.

Escuin, S., Navarro, R., & Fernandez, P. (2008). Fire severity assessment by using NBR (Normalized Burn Ratio) and NDVI (Normalized Difference Vegetation Index) derived from LANDSAT TM/ETM images. *International Journal of Remote Sensing*, *29*, 1053−1073.

Fernandez-Manso, O., Quintano, C., & Fernandez-Manso, A. (2009). Combining spectral mixture analysis and object-based classification for fire severity mapping. *Investigacion Agraria: Sistemas y Recursos Forestales*, *18*, 296−313.

Fox, D., Maselli, F., & Carrega, P. (2008). Using SPOT images and field sampling to map burn severity and vegetation factors affecting post forest fire erosion risk. *Catena*, *75*, 326−335.

French, N., Kasischke, E., Hall, R., Murphy, K., Verbyla, D., Hoy, E., & Allen, J. (2008). Using Landsat data to assess fire and burn severity in the North American boreal forest region: An overview and summary of results. *International Journal of Wildland Fire*, *17*, 443−462.

Garmin (2005). *Garmin eTrex Vista personal navigator*.Owner's manual and reference guide Available from: https://buy.garmin.com/shop/store/manual.jsp?product=010-00243-00&cID=167&pID=163 (Last visited on 24/02/2010).

Geerken, R., Zaitchik, B., & Evans, J. (2005). Classifying rangeland vegetation type and fractional cover of semi-arid and arid vegetation cover from NDVI time-series. *International Journal of Remote Sensing*, *24*, 5535−5554.

Gonzalez-Alonso, F., Merino-De-Miguel, S., Roldan-Zamarron, A., Garcia-Gigorro, S., & Cuevas, J. (2007). MERIS Full Resolution data for mapping level-of-damage caused by forest fires: the Valencia de Alcántara event in August 2003. *International Journal of Remote Sensing*, *28*, 789−809.

Hammill, K., & Bradstock, R. (2006). Remote sensing of fire severity in the Blue Mountains: Influence of vegetation type and inferring fire intensity. *International Journal of Wildland Fire*, *15*, 213−226.

Holben, B. (1986). Characteristics of maximum-value composite images from temporal AVHRR data. *International Journal of Remote Sensing*, *7*, 1417−1434.

Hudak, A., Morgan, P., Bobbitt, M., Smith, A., Lewis, S., Lentile, L., Robichaud, P., Clark, J., & McKinley, R. (2007). The relationship of multispectral satellite imagery to immediate fire effects. *Fire Ecology*, *3*, 64−90.

Isaev, A., Korovin, G., Bartalev, S., Ershov, D., Janetos, A., Kasischke, E., Shugart, H., French, N., Orlick, B., & Murphy, T. (2002). Using remote sensing to assess Russian forest fire carbon emissions. *Climatic Change*, *55*, 239−245.

Jain, T., Pilliod, D., & Graham, R. (2004). Tongue-tied. *Wildfire*, *4*, 22−26.

Jarvis, A., Reuter, H., Nelson, A., & Guevara, E. (2006). *Hole-filled seamless SRTM data V3*. Available from: http://srtm.csi.cgiar.org (Last visited on 24/02/2010.

Jonsson, P., & Eklundh, L. (2004). TIMESAT—A program for analyzing time-series of satellite sensor data. *Computers & Geosciences*, *30*, 833−845.

Ju, J., & Roy, D. (2008). The availability of cloud-free Landsat ETM+data over the conterminous United States and globally. *Remote Sensing of Environment*, *112*, 1196−1211.

Justice, C., Townshend, J., Vermote, E., Masuoka, E., Wolfe, R., Saleous, N., Roy, D., & Morisette, J. (2002). An overview of MODIS land data processing and products status. *Remote Sensing of Environment*, *83*, 3−15.

Kasischke, E., & French, N. (1995). Locating and estimating the areal extent of wildfires in Alaskan boreal forests using multiple-season AVHRR NDVI composite data. *Remote Sensing Environment*, *51*, 263−275.

Keeley, J. (2009). Fire intensity, fire severity and burn severity: A brief review and suggested usage. *International Journal of Wildland Fire*, *18*, 116−126.

Key, C. (2006). Ecological and sampling constraints on defining landscape fire severity. *Fire Ecology*, *2*, 34−59.

Key, C., & Benson, N. (2005). Landscape assessment: Ground measure of severity; the Composite Burn Index, and remote sensing of severity, the Normalized Burn Index. In D. Lutes, R. Keane, J. Caratti, C. Key, N. Benson, S. Sutherland, & L. Gangi (Eds.), *FIREMON: Fire effects monitoring and inventory systemGeneral Technical Report RMRS-GTR-164-CD LA*. (pp. 1−51) Rocky Mountains Research Station: USDA Forest Service.

Kutiel, P., & Inbar, M. (1993). Fire impacts on soil nutrients and soil erosion in a Mediterranean pine forest plantation. *Catena*, *20*, 129−139.

Landmann, T. (2003). Characterizing sub-pixel Landsat ETM+ fire severity on experimental fire in the Kruger National Park, South Africa. *South African Journal of Science*, *99*, 357–359.

Lee, B., Kim, S., Chung, J., & Park, P. (2008). Estimation of fire severity by use of Landsat TM images and its relevance to vegetation and topography in the 2000 Samcheok forest fire. *Journal of Forest Research*, *13*, 197–204.

Lentile, L., Holden, Z., Smith, A., Falkowski, M., Hudak, A., Morgan, P., Lewis, S., Gessler, P., & Benson, N. (2006). Remote sensing techniques to assess active fire characteristics and post-fire effects. *International Journal of Wildland Fire*, *15*, 319–345.

Lentile, L., Smith, F., & Shepperd, W. (2005). Patch structure, fire-scar formation, and tree regeneration in a large mixed-severity fire in the South Dakota Black Hills, USA. *Canadian Journal of Forest Research*, *35*, 2875–2885.

Lhermitte, S., Verbesselt, J., Jonckheere, I., Nackaerts, K., van Aardt, J., Verstraeten, W. W., & Coppin, P. (2008). Hierarchical image segmentation based on similarity of NDVI time series. *Remote Sensing of Environment*, *112*, 506–521.

Lhermitte, S., Verbesselt, J., Verstraeten, W. W., & Coppin, P. (2010). A pixel based regeneration index using time series similarity and spatial context. *Photogrammetric Engineering and Remote Sensing*, *76*, 673–682.

Lhermitte, S., Verbesselt, J., Verstraeten, W.W., Veraverbeke, S., & Coppin, P. Assessing intra-annual vegetation regrowth after fire using the pixel based regeneration index. *ISPRS Journal of Photogrammetry and Remote Sensing,* submitted for publication.

Li, M., Qu, J., & Hao, X. (2008). Detecting vegetation change with satellite remote sensing over 2007 Georgia wildfire regions. *Journal of Applied Remote Sensing*, *2*, 021505.

Lopez-Garcia, M., & Caselles, V. (1991). Mapping burns and natural reforestation using Thematic Mapper data. *Geocarto International*, *6*, 31–37.

Maselli, F. (2004). Monitoring forest conditions in a protected Mediterranean coastal area by the analysis of multiyear NDVI data. *Remote Sensing of Environment*, *89*, 423–433.

Miller, J., Knapp, E., Key, C., Skinner, C., Isbell, C., Creasy, R., & Sherlock, J. (2009). Calibration and validation of the relative differenced Normalized Burn Ratio (RdNBR) to three measures of fire severity in the Sierra Nevada and Klamath Mountains, California, USA. *Remote Sensing of Environment*, *113*, 645–656.

Miller, J., Safford, H., Crimmins, M., & Thode, A. (2008). Quantitative evidence of increasing forest fire severity in the Sierra Nevada and southern Cascade mountains, California and Nevada, US. *Ecosystems*, *12*, 16–32.

Miller, J., & Thode, A. (2007). Quantifying burn severity in a heterogenous landscape with a relative version of the delta Normalized Burn Ratio (dNBR). *Remote Sensing of Evironment*, *109*, 66–80.

Murphy, K., Reynolds, J., & Koltun, J. (2008). Evaluating the ability of the differenced Normalized Burn Ratio (dNBR) to predict ecologically significant burn severity in Alaskan boreal forests. *International Journal of Wildland Fire*, *17*, 490–499.

Olsson, L., & Eklundh, L. (1994). Fourier-series for analysis of temporal sequences of satellite sensor imagery. *International Journal of Remote Sensing*, *15*, 3735–3741.

Pausas, J. (2004). Changes in fire and climate in the eastern Iberian peninsula (Mediterranean Basin). *Climatic Change*, *63*, 337–350.

Pereira, J., Sa, A., Sousa, A., Silva, J., Santos, T., & Carreiras, J. (1999). Spectral characterization and discrimination of burnt areas. In E. Chuvieco (Ed.), *Remote sensing of large wildfires in the European Mediterranean Basin* (pp. 123–138). Berlin: Springer-Verlag.

Perez-Cabello, F., de la Riva Fernandez, J., Montorio Lloveria, R., & Garcia-Martin, A. (2006). Mapping erosion-sensitive areas after wildfires using fieldwork, remote sensing, and geographic information systems techniques on a regional scale. *Journal of Geophysical Research*, *111*, G04S10.

Polunin, O. (1980). *Flowers of Greece and the Balkans. A field guide* (pp. 1–592). Oxford: Oxford University Press.

Reed, B., Brown, J., Vanderzee, D., Loveland, T., Merchant, J., & Ohlen, D. (1994). Measuring phenological variability from satellite imagery. *Journal of Vegetation Science*, *15*, 703–714.

Riano, D., Moreno-Ruiz, J., Isidoros, D., & Ustin, S. (2007). Global spatial patterns and temporal trends of burned area between 1981 and 2000 using NOAA-NASA Pathfinder. *Global Change Biology*, *13*, 40–50.

Roder, A., Hill, J., Duguy, B., Alloza, J., & Vallejo, R. (2008). Using long time series of Landsat data to monitor fire events and post-fire dynamics and identify driving factors. A case study in the Ayora region (eastern Spain). *Remote Sensing of Environment*, *112*, 259–273.

Roy, D., Boschetti, L., & Trigg, S. (2006). Remote sensing of fire severity: Assessing the performance of the Normalized Burn Ratio. *IEEE Transactions on Geoscience and Remote Sensing*, *3*, 112–116.

Ruiz-Gallardo, J., Castano, S., & Calera, A. (2004). Application of remote sensing and GIS to locate priority intervention areas after wildland fires in Mediterranean systems: A case study from south-eastern Spain. *International Journal of Wildland Fire*, *13*, 241–252.

Savitzky, A., & Golay, M. (1964). Smoothing and differentiation of data by simplified least squares procedures. *Analytical Chemistry*, *36*, 1627–1639.

Song, C., & Woodcock, C. (2003). Monitoring forest succession with multitemporal Landsat images: Factors of uncertainty. *IEEE Transactions on Geoscience and Remote Sensing*, *41*, 2557–2567.

Specht, R. (1981). Primary production in Mediterranean-climate ecosystems regenerating after fire. In F. di Castri, D. Goodall, & R. Specht (Eds.), *Mediterranean-type shrublands* (pp. 257–267). Amsterdam: Elsevier.

Stow, D., Petersen, A., Rogan, J., & Franklin, J. (2007). Mapping burn severity of Mediterranean-type vegetation using satellite multispectral data. *GIScience & Remote Sensing*, *44*, 1–23.

Stroppiana, D., Pinnock, S., Pereira, J., & Gregoire, J. (2002). Radiometric analysis of SPOT-VEGETATION images for burnt area detection in Northern Australia. *Remote Sensing of Environment*, *82*, 21–37.

Teillet, P., Guindon, B., & Goodenough, D. (1982). On the slope-aspect correction of multispectral scanner data. *Canadian Journal of Remote Sensing*, *8*, 84–106.

Thomas, J., Walsh, R., & Shakesby, R. (1999). Nutrient losses in eroded sediment after fire in eucalyptus and pine forests in the wet Mediterranean environment of northern Portugal. *Catena*, *36*, 283–302.

Tobler, W. (1970). A computer model simulating urban growth in the Detroit region. *Economic geography*, *46*, 234–240.

Trabaud, L. (1981). Man and fire: Impacts on Mediterranean vegetation. In F. di Castri, D. Goodall, & R. Specht (Eds.), *Mediterranean-type shrublands* (pp. 523–537). Amsterdam: Elsevier.

van Leeuwen, W. (2008). Monitoring the effects of forest restoration treatments on post-fire vegetation recovery with MODIS multitemporal data. *Sensors*, *8*, 2017–2042.

Veraverbeke, S., Lhermitte, S., Verstraeten, W.W., & Goossens, R. (in press—a). Evaluation of pre/post-fire differenced spectral indices for assessing burn severity in a Mediterranean environment with Landsat Thematic Mapper. *International Journal of Remote Sensing*.

Veraverbeke, S., Verstraeten, W. W., Lhermitte, S., & Goossens, R. (2010). Illumination effects on the differenced Normalized Burn Ratio's optimality for assessing fire severity. *International Journal of Applied Earth Observation and Geoinformation*, *12*, 60–70.

Veraverbeke, S., Verstraeten, W., Lhermitte, S., & Goossens, R., (in press—b). Evaluation Landsat Thematic Mapper spectral indices for estimating burn severity of the 2007 Peloponnese wildfires in Greece. *International Journal of Wildland Fire*.

Verbesselt, J., Jonsson, P., Lhermitte, S., Jonckheere, I., van Aardt, J., & Coppin, P. (2006). Relating time-series of meteorological and remote sensing indices to monitor vegetation moisture dynamics. In C. Chen (Ed.), *Signal and image processing for remote sensing* (pp. 153–173). Darmouth: CRC press.

Verbyla, D., Kasischke, E., & Hoy, E. (2008). Seasonal and topographic effects on estimating fire severity from Landsat TM/ETM+ data. *International Journal of Wildland Fire*, *17*, 527–534.

Vermote, E., El Saleous, N., & Justice, C. (2002). Atmospheric correction of MODIS data in the visible to middle infrared: First results. *Remote Sensing of Environment*, *83*, 97–111.

Verstraete, M., & Pinty, B. (1996). Designing optimal spectral indexes for remote sensing applications. *IEEE Transactions on Geoscience and Remote Sensing*, *34*, 1254–1265.

Viedma, O., Melia, J., Segarra, D., & Garcia-Haro, J. (1997). Modeling rates of ecosystem recovery after fires by using Landsat TM data. *Remote Sensing of Environment*, *61*, 383–398.

Viovy, N. (2000). Automatic classification of time series (ACTS): A new clustering method for remote sensing time series. *International Journal of Remote Sensing*, *21*, 1537–1560.

White, J., Ryan, K., Key, C., & Running, S. (1996). Remote sensing of forest fire severity and vegetation recovery. *International Journal of Wildland Fire*, *6*, 125–136.

Wolfe, R., Roy, D., & Vermote, E. (1998). MODIS land data storage, gridding, and compositing methodology: Level 2 grid. *IEEE Transactions on Geosciences and Remote Sensing*, *36*, 1324–1338.

Zhu, Z., Key, C., Ohlen, D., & Benson, N. (2006). Evaluate sensitivities of burn-severity mapping algorithms for different ecosystems and fire histories in the United States. *Final Report to the Joint Fire Science Program: Project JFSP 01-1-4-12* (pp. 1–36). Sioux Falls, SD: US Department of Interior.